Transcriptome profile of the zebrafish atrioventricular canal reveals molecular signatures of pacemaker and valve mesenchyme

Abu Nahia Karim[1], Migdał Maciej[1], Quinn T. Alexander[4], Poon Kar-Lai[2,3], Łapinski Maciej[1], Sulej Agata[1], Pawlak Michał[1], Bugajski Łukasz[5], Piwocka Katarzyna[5], Brand Thomas[3], Kohl Peter[6,7], Korzh Vladimir[1†], Winata Cecilia[1,8†]

[1]International Institute of Molecular and Cell Biology in Warsaw, Warsaw, Poland

[2]Institute of Molecular and Cell Biology, Singapore

[3]Developmental Dynamics, National Heart and Lung Institute, Imperial College London, London, United Kingdom

[4]Department of Physiology and Biophysics, Dalhousie University, Canada

[5]Nencki Institute of Experimental Biology, Warsaw, Poland

[6]Cardiac Biophysics and Systems Biology, National Heart and Lung Institute, Imperial College London, London, United Kingdom

[7]Department of Computer Science, University of Oxford, United Kingdom

[8]Max Planck Institute for Heart and Lung Research, Bad Nauheim, Germany

[†]To whom correspondence should be addressed

Keywords: atrioventricular canal, atrioventricular node, cardiac valve, cardiac pacemaker, zebrafish, RNA-seq

Abstract

The atrioventricular canal (AVC) is an essential feature of the heart, which separates the atrium from the ventricle. During heart morphogenesis, it is a hub of molecular processes necessary for distinguishing heart regions; most importantly, for the formation of the AV conduction system and cardiac valves. To better understand the molecular processes underlying AVC development and function, we utilized the transgenic zebrafish line *sqet31Et* with EGFP expression in the AVC region to isolate this cell population by FACS and profiled its transcriptome by RNA-seq at 48 and 72 hours post fertilization (hpf). Compared to the rest of the heart, the AVC is enriched for the expression of molecular markers associated with mammalian AVC and AV node, including *cx36.7* and *cx45* which encode connexins forming low conductance gap junctions. Using the transgenic line *Tg(myl7:mermaid)* encoding the voltage-sensitive fluorescent protein, we showed that loss of function of Isl1 abolished the pacemaker-containing sinoatrial ring (SAR) and resulted in an erratic spread of excitation pattern from the SAR to AVC, indicating the dysfunction of the primary pacemaker. Concurrently, ectopic excitation in the AVC region was observed, suggesting that the zebrafish AVC possesses inherent automaticity although insufficient to replace the primary pacemaking activity of the SAR. Comparisons between the SAR and AVC transcriptomes revealed partially overlapping expression profiles of various ion channels and gap junction proteins which reflects their diversified functions. Lastly, we observed dynamic expression of epithelial-to-mesenchymal transition markers, as well as components of TGF-β, Notch, and Wnt signaling pathways, which have been implicated in the formation of AVC conduction and cardiac valves. Our results uncovered the molecular hallmarks of the developing AVC region and demonstrated its role in the structural and electrophysiological separation between the atrium and ventricle.

Author summary

The atrioventricular canal is a structure in the embryonic heart which separates the atrium from the ventricle. It gives rise to the AV node and cardiac valves - two important structures which ensure unidirectional blood flow between heart chambers. The AV node serves to regulate the propagation of electrical impulses between the two chambers, such that they contract consecutively. Using the zebrafish as model organism, we performed gene expression profiling and characterized electrical conduction patterns between the sinoatrial primary pacemaker and AVC. We discovered that the zebrafish AVC possesses similar features to the mammalian AV node, including slow conduction, inherent pacemaking activity, and the expression of conserved developmental genes. The molecular profile of the AVC is distinct from that of the sinoatrial pacemaker, which reflects their distinct roles. In addition, we found that genes regulating cardiac valve development were also expressed in the AVC, illustrating the importance of this region for establishing both electrophysiological and structural separation between the heart chambers. Besides establishing conserved aspects between zebrafish and mammalian conduction system, the data generated in this study constitutes a valuable resource for studying AVC development and discovery of novel candidate genes implicated in regulating cardiac rhythm and cardiac valve formation.

Introduction

The atrioventricular canal (AVC) serves two critical purposes in cardiac development and function. Firstly, the AVC gives rise to the AV node, which constitutes part of the cardiac conduction system (CCS) responsible for generating and transmitting electrical impulses necessary for coordinated heart contraction [1,2]. In the mammalian heart, the AV node can be found within the interatrial septum, at the AV junction [3]. The AV node constitutes a group of cells regulating the transmission of electrical impulses between cardiac chambers. Electrical impulses originating from the sinoatrial (SA) node are delayed by a fraction of a second in the AV node before being propagated to the ventricle. Such delay ensures consecutive contractions

of the atrium and ventricle [4]. In the mature, 4-chambered murine heart, the AV node serves as the only region of continuity between atrial and ventricular myocardium. It is surrounded by low-conducting fibrous tissue known as the annulus fibrosus, which derives from the epicardium and acts as an insulator between the atrial and ventricular myocardium [5]. The AV node is also often referred to as a secondary pacemaker as it possesses intrinsic automaticity, which renders it a potential arrhythmogenic source in cases where weakened or abnormal impulses from the SA node are not able to override it [3,6,7].

In the mammalian embryonic heart, the AV myocardium is slow conducting, unlike chamber myocardium. This property is retained in those cells that become the future AV node in the adult heart [2]. These cells express *Bmp4*, *Tbx2*, and *Tbx3*, which suppress the genetic program leading to the specification of working cardiomyocytes [8–10]. The electrophysiological properties of the AV node are determined by several factors, mainly the electrical coupling between its cells mediated by gap junctions. Connexins form gap junctions by either homogenous or heterogeneous pairings, resulting in a different range of conductivity [11,12]. In the mammalian heart, CX30.2 and CX45 form low or ultra-low conductance gap junctions and are enriched in AV pacemaker cells [13,14]. CX43 typically forms medium conductance gap junctions in the working myocardium [15,16]. It can also form low-conductance gap junctions by pairing with lower conduction connexins such as CX30.2 [17].

In zebrafish, the earliest indication of a functional AV-node-like region in the heart was observed through calcium wave imaging, which revealed significant conductance delay between the atrium and ventricle from 36 hpf [18]. Notch1b and Neuregulin expressed in the endocardium have been shown to be involved in the development of this conduction delay [19]. To date, no live markers of the pacemaker have been available for direct visualization of its morphology and structure, or isolation for molecular characterization. Zebrafish orthologs of

Tbx2, and *Tbx3* are expressed in the region that corresponds to the AVC in the mammalian heart [20,21]; however, no detailed analyses have been made to elucidate the molecular profile of this structure, nor confirm its homologous function to the mammalian AV node. The LIM-homeodomain transcription factor (TF) Islet1 (Isl1) [22–24] was found to play a role in the development of the primary pacemaker, the SA node, as its deficiency causes cardiac arrhythmia [21,25]. Isl1-positive cells in the sinoatrial region (SAR) of adult zebrafish co-expresses *hcn4*, which encodes the hyperpolarization-activated channel responsible for generating the pacemaker current (I_f) [26]. In the AVC of adult zebrafish, a small group of *hcn4*-positive cells was found in the AV valves. However, in contrast to the SAR, Hcn4-positive cells in the AVC region were Isl1-negative [27]. The earliest expression of *hcn4* in zebrafish embryonic AVC was reported from 52 hpf [28], which suggests that it could potentially function as a secondary pacemaker. Electrical silencing of cells in the SAR region of the embryonic zebrafish heart using optogenetics abolished the heartbeat, which suggests that the activities of alternative pacemaker regions, such as the AVC, are not sufficient to drive heart contractions [29]. Interestingly, surgical isolation of the ventricle from the atrium led to the establishment of the AV region as the site of electrical activation origin, which revealed its ability to function as a secondary pacemaker although with a slower excitation rate [27].

Besides its role in cardiac conduction, the AVC gives rise to the atrial and ventricular septa, which provide structural division between the four chambers of the mammalian heart. These structures also include the primary cardiac valves: the mitral and tricuspid valves. Studies in various model organisms have revealed the stepwise processes in AVC development, including its early patterning, endocardial cushion formation, and valve maturation [2,30]. During cardiac chamber formation, a layer of extracellular matrix known as the cardiac jelly separates the myocardium from the endocardium. The cardiac jelly subsequently disappears from the chamber-forming regions, while being retained at the AVC region. Signals from

the myocardium induce the endocardial cells to undergo epithelial-to-mesenchymal-transition (EMT), a process where epithelial cells undergo changes in cell polarity and cell-cell adhesion properties and are converted to migratory mesenchymal cells [31]. These cells populate the underlying cardiac jelly, becoming the mesenchyme substrate [32], which forms the endocardial cushions. These cushions continue to grow, forming the septa separating ventricles and atria, as well as valve leaflets. TGF-β signaling is known to play a role in endocardial cushion formation by promoting EMT [33]. In addition, Notch, Wnt, and BMP signaling activities in AVC endocardium and myocardium are also crucial to regulate the formation of endocardial cushion and valve [34].

In the zebrafish heart, AVC formation is initiated as early as 30 hpf when a constriction between the atrium and ventricle separates the two chambers as the heart begins to loop. At the same time, endocardial cells at the A-V border start becoming cuboidal in shape, and cardiomyocytes in the same region adopt a trapezoid morphology with a wider basolateral surface. These cells express higher levels of the surface adhesion molecule *alcama* compared to working cardiomyocytes [35]. Around the time when heart looping is initiated at 36 hpf, *bmp4* expression becomes restricted to the AVC myocardium [36], where it plays a role in the formation of cardiac jelly together with Has2 [37]. The development of valves is initiated by the formation of endocardial cushions at two opposite sides of the AVC at 55 hpf [35]. By 60 hpf, some of these endocardial cells migrate into the underlying cardiac jelly and undergo EMT, which provides the substrate for valve development [35]. Canonical Wnt signaling is required for zebrafish endocardial cushion formation [38,39], although its precise mechanism is still unknown. In addition, Wnt signals originating from the endocardium induce myocardial *bmp4* and *tbx2b* expression, which are necessary for patterning the AVC myocardium [40]. Similarly, *notch1b* and its ligand *dll4* are expressed in the AVC endocardium [34,36] and are required for the formation of the endocardial cushion as well as AV conduction tissue [35,41].

Given its important role in the formation of major cardiac structures, disruptions to AVC development can result in various forms of septal defects, as well as valve abnormalities leading to heart failure. In addition, defects of the AV node may lead to various degrees of AV block, which gives rise to cardiac arrhythmia [42]. However, despite its importance, our knowledge of genetic events responsible for the development and function of the AVC region in general, as well as of the AV node in particular, is still limited. One of the main challenges in studying the AVC is posed by their complex spatial anatomy and cellular heterogeneity [43]. For this reason, isolation of specific cell populations from ambient working myocardium and other surrounding tissues is challenging, which limits the identification of clear-cut molecular markers. Moreover, functional genetic studies of the AVC in higher vertebrates are impractical due to the early embryonic lethality caused by loss of function of essential genes. Thus, there is still a lack of a good and established system that can reliably model the development, physiology, and pathology of the AVC.

Despite the significant evolutionary distance between human and zebrafish, the zebrafish heart is remarkably similar to the human heart in terms of basal heart rate, electrophysiological properties, and action potential shape and duration [44,45]. Several zebrafish mutants for cardiac ion channels have been described, which display phenotypes closely resembling those found in various forms of human arrhythmia [46–48]. In addition, relevant phenotypes have also been shown to result from transgenic expression of human disease mutations, which illustrates the high conservation of molecular pathways regulating electrical conduction in the heart [49]. The zebrafish therefore holds great potential to model human pathologies affecting the AVC and AV pacemaker function.

An enhancer trap screen performed in zebrafish has generated a collection of transgenic lines expressing enhanced green fluorescent protein (EGFP) in different tissues or subdomains of the

heart [44,50]. Among these lines, two express EGFP either in the SAR or AVC. The transgenic line *sqet33mi59BEt*, in which the enhancer trap was inserted close by the *fhf2* gene locus, expresses EGFP in the SAR [51]. Recently, we completed the analysis of the transcriptome of these cells [52]. The transgenic line *sqet31Et* exhibits green fluorescent protein (GFP) expression in a ring structure in the region of the AVC [50], which corresponds to the ring of AV conduction tissue as described previously [18,19]. Here we utilize the *in vivo* labeling of the AVC in the transgenic line *sqet31Et* to isolate cells making up this structure and perform detailed molecular characterization by transcriptome profiling at 48 hpf and 72 hpf, corresponding to the time of CCS and cardiac valve development. To better understand the physiology of the CCS in zebrafish, we characterized the electrical conduction patterns between the SAR and AVC, and cross-compared the transcriptome profiles of both pacemaker regions. Our results show that the AVC gene expression profile exhibits hallmarks of the mammalian AV node and reflects ongoing biological processes implicated in valve development. Comparisons between the SAR and AVC transcriptomes revealed differences reflected in expression profiles of ion channels and connexins implicated in pacemaker function. This data constitutes a valuable resource for the study of AVC development and function and identification of candidate genes implicated in these processes.

Results

Transgenic zebrafish line *sqet31Et* expresses EGFP in the zebrafish AVC

The *sqet31Et* transgenic line expresses EGFP in a ring structure marking the AVC, which likely corresponds to slow conducting myocytes homologous to the mammalian AV node [18,19,50,51]. To better visualize this structure, we performed high resolution imaging at 48 hpf and 72 hpf (Fig. 1A-D). To mark the myocardium, we crossed *sqet31Et* with *Tg(myl7:mRFP)* that expresses membrane-bound RFP (mRFP) in cardiomyocytes. Confocal

imaging of the AVC region revealed that at the surface of the AVC, the EGFP and mRFP expression overlapped, confirming the myocardial nature of the EGFP-expressing cells (Fig. 1C). At 72 hpf, two additional groups of ~3 cuboidal-shaped cells were detected at the deeper layer facing the cardiac lumen (Fig. 1D). These cells appear to be a part of the characteristic protrusion into the cardiac lumen most likely representing the developing atrioventricular cushion. Based on their location between the endocardium and myocardium, these cells have been previously defined as constituents of the non-chamber valve tissue [50,51]. An additional EGFP expression domain detected previously [50] was observed at the bulbus arteriosus (BA, corresponding to the mesenchyme of the outflow tract in mammals [53]) from 72 hpf (Fig. 1B). The EGFP expressing domain in the developing heart of the *sqet31Et* transgenic line thus consists of largely AVC myocardium, with another expression domain in the BA, the latter observed only at 72 hpf.

Transcriptome profile of the AVC

To characterize the molecular profile of the GFP+ cell population in *sqet31Et*, we isolated these cells using fluorescence-activated cell sorting (FACS) at 48 hpf and 72 hpf (Fig. 2A) and profiled their transcriptome by RNA-seq. The rest of the heart cells, which did not express EGFP, were also collected (GFP-). Average sequencing reads mapping to the *egfp* sequence were considerably higher in GFP+ compared to GFP- samples, confirming the high representation of the EGFP-expressing cell population in the GFP+ samples (S1 Figure B). Principal component analysis (PCA) revealed the tight clustering of replicates and clear separation between sample types (Fig. 2B). Moreover, samples of the same developmental stages clustered closer together, indicating their similarity to each other.

To identify genes enriched in the GFP+ cell population compared to the rest of the heart, we performed differential expression analysis of the GFP+ against GFP- fractions. In both

219 developmental stages, a total of 3798 and 2777 genes were differentially expressed at 48 hpf
220 and 72 hpf, respectively (absolute log2FC > 2, padj < 0.05), of which 1492 were common
221 for both stages (Fig. 2C, F, S2 Table). GO and KEGG pathway enrichment analyses at 48 hpf
222 revealed that the set of genes overexpressed in GFP+ compared to GFP- cells (enriched genes)
223 was overrepresented for functional terms related to cardiac muscle development and function
224 ("cardiac muscle contraction", "adrenergic signaling in cardiomyocytes", "cardiac muscle
225 development", "cardiac muscle differentiation", and "calcium signaling pathway"),
226 which supports the myocardial identity of the GFP+ fraction (Fig. 2D, E, S3 Table).
227 On the other hand, functional terms related to cell-cell adhesion ("cell adhesion molecules",
228 "cell-cell adhesion") were overrepresented among transcripts overexpressed in the GFP- cell
229 population. At 72 hpf, similar functional terms were overrepresented with the addition
230 of "vascular smooth muscle contraction" term (Fig. 2G, H, S3 Table), which likely corresponds
231 to the initiation of EGFP expression in the BA at this stage.

232 To assess whether the sorted GFP+ fraction contained AVC cells, we explored the presence of
233 known markers of AVC in our dataset. We established a set of AVC marker genes for zebrafish
234 and mammals by retrieving genes annotated with the term "atrioventricular canal" from
235 the ZFIN (http://zfin.org/) and MGI [54] gene expression databases. Intersection of these known
236 markers with the set of AVC-enriched transcriptome returned 46 and 58 genes in common,
237 which were enriched in GFP+ cells at both 48 hpf and 72 hpf, respectively (Fig. 3A, B; S4
238 Table). Notably, several of these genes were known to be expressed specifically in zebrafish
239 AVC myocardium, including *bmp4* [36], *wnt2bb* [55], *snai1b* [56], *hey2* [57], and *hnf1ba* [18].
240 On the other hand, 27 genes which were enriched in the GFP- population overlapped known
241 AVC markers at either or both developmental stages. These included *id4* and *notch1b* reported
242 to be expressed in the endocardium [41,58], which suggests that the GFP+ cells in *sqet31Et* are
243 less likely to be endocardial. Whole mount *in situ* hybridization of eight selected AVC-enriched

transcripts with no previous heart expression data further confirmed their expression in the AVC except for one, *si:dkey-57k2.6*, which is expressed only in the BA. Another transcript, *si:dkey-164f24.2*, was expressed in the whole heart (S2 Figure). Therefore, utilizing the *sqet31Et* transgenic line to specifically enrich for the GFP+ cell population, our RNA-seq analysis revealed the transcriptome mainly representing the AVC, with contribution from the BA.

AVC gene expression profile shows signatures of AV pacemaker

Our transcriptome analyses revealed several key features of the zebrafish AVC. Firstly, a hallmark feature of mammalian AVC myocardium is its slow conduction in contrast to chamber myocardium. Among the transcripts enriched in the GFP+ cell population, we found 10 encoding various connexins. These consisted of *cx36.7* (ortholog of human CX31.9 and murine Cx30.2; [59,60]) and *cx43.4/cx44.2* (ortholog of human CX45; [60]), whose mammalian orthologs form low or ultra-low conductance gap junctions in the AV node [13,14,61]. These were enriched in the GFP+ population at both developmental stages, while other connexin transcripts were enriched only at 48 hpf (padj < 0.05). The latter group consisted of *cx28.9/cx32.3* (ortholog of human CX37; [60]), *cx43*, and *gja3/cx46* (Fig. 3C; S5 Table). Among those with the highest fold-change between the GFP+ and GFP- cell populations were *cx36.7*, *gja3/cx46*, and *cx32.3* at 48 hpf and *cx36.7* at 72 hpf. Loss of function of mammalian CX46 leads to cardiac conduction disorders, while the loss of *gja3/cx46* in the zebrafish mutant *dco* causes defects in heart morphology and ventricular conduction pattern [62]. The enrichment of genes encoding connexins able to form low conductance gap junctions likely reflects the conduction delaying property of the AVC region. Besides those known for their role in cardiac conduction, transcripts encoding other members of the connexin family [Cx30.3 (CX30), Cx34.4 (CX30.3) and Cx35.4 (CX31)] were also enriched in the GFP+ cell

268 population. These have not been previously implicated in heart or pacemaker function and are
269 candidates for further investigation.

270 Besides delaying electrical conduction between the atrium and ventricle, the mammalian
271 AV node also possesses intrinsic pacemaker activity [3,6]. We thus searched amongst the AVC-
272 enriched gene list for those known to be expressed in the AV node or associated with pacemaker
273 development and function (S6 Table; [63–66]. Confirming previous reports [28], the expression
274 of *hcn4* was observed in the GFP+ cell population at both 48 hpf and 72 hpf (S3 Figure;
275 S6 Table). In addition, genes encoding zebrafish orthologs of transcription factors known to
276 be involved in mammalian pacemaker cell specification [67–69] were expressed in the GFP+
277 population (*tbx18, shox2, tbx2a, tbx2b,* and *tbx3*; S3 Figure, S6 Table). In mammalian CCS,
278 the transcription factors Tbx2 and Tbx3 are known to repress the expression of the chamber-
279 specific Cx40 [67,70]. In agreement with this, *gja5a/b* (the zebrafish ortholog of CX40),
280 was not AVC-enriched. It has been shown that *nkx2.5* is expressed in all myocardium,
281 but slightly higher in the AV conduction system [64]. Similarly, we found that *nkx2.5*
282 was enriched in GFP+ cells compared to GFP- at 48 hpf (S3 Figure, S6 Table). Taken together,
283 the transcriptome of AVC myocardium reveals conserved features to that of the mammalian
284 AV node in terms of expression of genes linked to slow conductivity, automaticity,
285 and molecular mechanism for AV node specification. Therefore, our results support the notion
286 that the AVC is a homologous structure to the mammalian AV node and suggest that the core
287 network leading to the specification of the AV conduction system is conserved between
288 mammals and fish.

289 **Defect of the primary pacemaker in the SAN reveals spontaneous activity of the AVC**
290 **pacemaker**

The expression of *hcn4* and other markers in AVC, suggesting its homology to the mammalian AV node, led us to question whether the zebrafish AVC possesses inherent pacemaking activity as does its mammalian counterpart. To this end, we utilized the *isl1* K88X mutant (*isl1*^{sa29}), which has been shown to exhibit a defective SAR pacemaker function that manifests as sinus pauses and bradycardia [21,25]. We observed that, apart from losing the expression of *fhf2a* (Fig. 4A, B), *bmp4* (Fig. 4C, D), and the pacemaker marker *hcn4* (Fig. 4E, F) in the sinus venosus, the *isl1* mutant was also devoid of EGFP-positive cells at the SAR, but not the AVC, as shown by analysis of *sqet33mi59BEt* and *sqet31Et*, respectively (Fig. 4G, H). Hence, we confirmed that the reduced number of cardiomyocytes at the venous pole in *isl1*$^{-/-}$ observed previously [25] resulted from the absence of the pacemaker cells-containing SAR. It is worth noting that the *isl1*$^{-/-}$ is the only vertebrate mutant that shows a complete lack of pacemaker SAR cells. In support of this, Isl1 overexpression resulted in a small increase in the fluorescence intensity of EGFP-expressing pacemaker cells in *sqet33mi59BEt* at 40 hpf (Fig. 4I, J).

Despite the complete absence of the SAR pacemaker, Isl1-deficient hearts contract, albeit inefficiently and irregularly, with long pauses (Fig. 5A, C, Supplementary movies 1 and 2). This suggests the existence of alternative origins of automaticity that triggers the initiation of cardiac contractions. To investigate whether the AVC could generate electrical impulses independent of the SAR, the Isl1 antisense morpholino [71] was injected into 1-4 cell stage zebrafish embryos expressing the genetically encoded voltage-sensitive fluorescent protein Mermaid, *Tg(myl7:mermaid)*. This allowed direct observation of cardiac electrical conduction patterns. Similar to *isl1* mutants, about 66% of Isl1 morphants showed sinus pauses (6 of 9 morphants *vs* 4 of 6 mutants), and all showed bradycardia. The heart rate of Isl1 morphants was 80.2±15 beats per minute (bpm) at 48 hpf (mean ± SEM., n=6) and 141,2±10.3 bpm at 72 hpf, (n=6), which is significantly lower than that in controls (176±5.7 bpm at 48 hpf, (n=7) and

315 229±6.6 bpm at 72 hpf, (n=18)) (Fig. 5A). Increased variability in heartbeat duration was noted
316 in the Isl1 morphants as well.

317 Optical mapping showed that in control hearts, the excitation wave front travelled uniformly
318 across the atrium from the SAR towards the AVC (Supplementary movie 1; Fig. 5B).
319 In contrast, in Isl1 morphants, atrial excitation, although predominantly originating from
320 the SAR region, became uncoordinated (Supplementary movie 2; Fig. 5B). During the sinus
321 pause, several stationary centers of automaticity distributed from posterior to anterior were
322 detected, with the SAN-associated location showing the highest activity. Interestingly,
323 the location associated with AVC became more active near the end of the atrial contraction
324 (Supplementary movie 2, Fig. 5B, asterisk), presumably when triggering the consecutive phase
325 of the contraction cycle in the ventricle. The activity of the AVC location became even more
326 pronounced during the periods of sinus pause. The loss of coordinated atrial excitation
327 and conduction in Isl1 deficient embryos therefore suggests that the SAR is the primary
328 pacemaker required for coordination of atrial excitation. However, coordinated ventricular
329 excitation can be induced by the electrical activity of the AVC, in particular when no wave of
330 excitation from the SAR drives the heartbeat. Inherent AVC pacemaker rate is lower than that
331 of the SAR.

332 **Comparison between the AVC and SAR transcriptomes reflect distinct**
333 **electrophysiological properties**

334 The observation that both SAR and AVC regions of the zebrafish heart possess pacemaker
335 activity, albeit at different inherent rates, led us to question the molecular nature underlying
336 their distinct properties. To this end, we compared the transcriptome of the AVC with that
337 of the SAR [52] to identify differentially enriched genes. We re-analyzed the SAR dataset to
338 identify SAR-enriched genes and intersected this with our AVC-enriched gene list (S2 Table),

obtaining a total of 1516 AVC-unique and 701 SAR-unique genes, and 450 genes common between the two (S7 Table). Notably, several genes encoding proteins involved in ion transport, cell junction formation, and extracellular matrix were differentially enriched between the AVC and SAR.

Interestingly, the expression of *hcn4* was significantly higher in the SAR, while not significantly higher in the AVC, compared to the rest of the heart. This may reflect the role of SAR as the dominant pacemaker (S7 Table). In addition to *hcn4*, several other transcripts encoding various ion channels were enriched in both the SAR and AVC, notably, the T-type calcium channel Cacna1g, which is necessary for mammalian pacemaker activity in both SA and AV nodes [72]. Those genes enriched in AVC and not the SAR include *trpm4* encoding a Ca^{2+}-activated nonselective cation channel, which mediates cell membrane depolarization [73]. TRPM4 is implicated in human progressive familial heart block type I characterized by cardiac conduction blockage downstream of the AV node [74]. Another notable example is *cacna1c*, whose human ortholog is associated with the Wolff-Parkinson-White syndrome [75], a condition affecting the AV conduction system [76]. Other genes, including *kcnq1.1*, *kcne4*, and *atp1b1a*, possess human orthologs associated with the maintenance of QT interval [77–79].

Despite having some common properties, the SA and AV nodes perform distinct functions. The SA node serves a primarily pacemaking function, while the AV node is mainly specialized to delay electrical propagation between the atrial and ventricular chambers [11]. Therefore, while both regions express partially overlapping, mostly low-conducting, gap junction proteins [11,80], the AV node is particularly enriched in Cx30.2 and Cx45 [61,81,82]. In line with this, *cx36.7*, the zebrafish paralog of *Cx30.2*, was enriched in the AVC but not the SAR (S7 Table). On the other hand, *cx43.4*, a paralog of *Cx45*, was enriched in both the SAR and AVC (S7 Table). Low electrical coupling is also a necessary property within the definitive pacemaker

cells of the SA node to prevent inhibitory interference from the surrounding working myocardium, which is more hyperpolarized [11]. Collectively, the overall differences in ion channel, cell adhesion, and extracellular matrix composition enriched in the SAR and AVC likely underlie their distinct electrophysiological properties.

Developmental signaling pathways dynamics suggests signaling interaction between AV myocardium and endocardial cells during valve formation

Besides hosting the AV node, the AVC is also the site of valve formation. We identified transcripts encoding genes involved in the EMT process enriched in the GFP+ compared to GFP- cell population (Fig. 6A, B; S8 Table). These include 22 genes enriched at both developmental stages and 28 genes enriched only at either the 48 hpf or 72 hpf stage. Members of the TGF-β signaling pathway were enriched in GFP+ cells at both developmental stages (*tgfb2, tgfb1a, smad1, smad6b, and smad9*) (Fig. 6C - E). In addition, the GFP+ enrichment of *tgfb3, tgfbr2b,* and *smad6a* in GFP+ cells was specific to the 48 hpf stage (Fig. 6C). This is in line with the observation in mammalian endocardial cushion formation, where various TGF-β ligands are expressed in different cell populations of the AVC: TGF-β1 in endocardium, TGF-β2 in myocardial and endocardial cells flanking the cushions, and TGF-β3 in the cushion mesenchyme [83].

Notch signaling activity in the AVC endocardium is necessary for the initiation of the EMT process by activating SNAI1 and SNAI2 expression [84,85]. Transcripts encoding key components of the Notch pathway were enriched in GFP+ cells at both developmental stages. These include *jag1b*, *hey1*, and *hey2*, and *prss23*, implicated in AV valve formation [86]. On the other hand, *jag1a, jag2a, her6, jagn1b, notch2,* and *notch3* were enriched at either stage (S2 Table). In contrast, valve endocardial markers *notch1b* and its ligand *dll4* [34–36] were not enriched in GFP+ cells, which further supports the non-endocardial identity of this population.

Several components of the canonical Wnt signaling have been reported to be expressed in different cell layers of the mammalian AVC, including *Wnt2*, *Fzd2*, and *Lef1* in the cushion mesenchyme and *Wnt4* and *Wnt9b* in endocardial endothelium [87]. In agreement with this, we found that, in the zebrafish AVC, *wnt2bb* was enriched in GFP+ cells at both stages, while *wnt7ab*, *wnt6b*, *wnt5a/b*, and *wnt4* were enriched only in 48 hpf (Fig. 6C - E). On the other hand, *fzd7a/b* and *fzd9a/b* encoding Wnt signaling receptors were enriched in both stages, *fzd2* and *fzd6* enriched only at 48 hpf, while *fzd6*, *fzd8a*, and *fzd10* only at 72 hpf (Fig. 6C-E). Whereas *dkk1a/b* and *dkk2* encoding Wnt antagonists were enriched only at 48 hpf. Interestingly, we observed that at 72 hpf, except for *wnt2bb*, no transcripts of Wnt ligands were enriched in GFP+ cells, while transcripts encoding several Frizzled family receptors and downstream components were enriched (Fig. 6D). To visualize Wnt signaling activity in the AVC region, we crossed the *sqet31Et* transgenic line with the Wnt reporter line *Tg(7x TCF-Xla.Sia:NLS-mCherry)* [88]. In agreement with previous reports of the presence of Wnt signaling in the AVC myocardium [40,89], we observed that both the non-EGFP-expressing endocardium and EGFP-expressing cells had Wnt signaling activity at all developmental stages (S4 Figure).

The process of valve development is reflected in the dynamics of signaling pathway activity occurring between the early and late stages of AVC development. We found a total of 5877 genes differentially expressed at 72 hpf compared to 48 hpf (padj < 0.05; -1 < log2FC > 1; S5 Figure, S9 Table). Notably, GO terms related to TGF-β, Wnt, and Notch signaling pathways were overrepresented at 72 hpf (S10 Table). Many members of these three signaling pathways exhibited dynamic expression between 48 hpf and 72 hpf (S5 Figure; S11 Table). Collectively, our observations uncover the dynamic expression of various components of the TGF-β, canonical Wnt, and Notch signaling pathways in the AVC myocardium, which likely reflects their role in the ongoing AVC patterning and valve development.

AVC-enriched genes are associated with human congenital heart defects related to CCS, valves and septa

We identified the human orthologues of AVC-enriched genes and interrogated them for any association with clinical phenotypes related to ClinVar terms: “arrhythmia”, “AV block”, “long QT syndrome”, and “conduction”. Our analysis revealed a total of 91 and 60 unique genes associated with these four ClinVar terms at 48 hpf and 72 hpf stages, respectively (S12 Table). Specifically, the disease conditions represented by these terms included more general forms of cardiac arrhythmia such as atrial fibrillation, sick sinus syndrome, abnormal QT interval, and Brugada syndrome, as well as those conditions specifically associated with defects of the AV conduction system or downstream effects such as heart block [90], Wolff-Parkinson-White pattern [76], and supraventricular tachycardia [91]. The latter group included *trpm4* and *cacna1c*, which were enriched in both SAR and AVC, as well as *mybpc3, smyhc2, hrc, dspa, myh7l, zgc:86709, lmna, snta1*, and *ttn.2*.

As the AVC is also the site where the endocardial cushion and valve develops, we expected to find associations between AVC-enriched genes and human valve and septal defects. We searched the human orthologues of AVC-enriched for overlap with ClinVar terms containing “tricuspid valve”, “AV valve”, “mitral valve”, and “valve in general”. In total, 115 and 93 unique genes were associated with these terms at 48 hpf and 72 hpf, respectively (S13 Table). In addition, we also searched for those associated with the ClinVar term “septal defect” and obtained 66 and 55 unique genes associated with the term at each stage, respectively (Supplementary Table 14). In the adult human heart, the AV node is embedded into the interatrial septum [3]. Given that the endocardial cushions are involved in the formation of the AV valves and septa, it comes as no surprise that the defects of interatrial septum could be linked to defects in cardiac conduction. In fact, a number of genes were commonly associated with ClinVar terms “cardiac conduction” and “valve” (S14 Table). For example, *tbx5a*, whose

human orthologue TBX5 causes the Holt-Oram syndrome characterized by congenital heart malformation due to variable atrial and ventricular septal defects as well as heart conduction defects [92,93]. Another notable example is *smyhc2*, whose human orthologue MHY6 is associated with both atrial septal defect and sick sinus syndrome [94,95]. Other examples include *cacna1c*, *ttn.2*, *snta1*, *lmna*, *dspa*, and *mybpc3*. Taken together, the overlap of a large number of AVC-enriched genes with human heart conditions related to CCS and valve/septal defects suggests our transcriptomics data as a valuable resource for studying these diseases.

The bulbus arteriosus transcriptome contributes to a set of differentially expressed genes at 72 hpf

Among the GO terms associated with a set of genes enriched at 72 hpf is "Vascular smooth muscle contraction". This term likely reflects the expression of EGFP in the BA at 72 hpf. The BA is a teleost-specific structure, which exists in place of the outflow tract of higher vertebrates [53]. Unlike the outflow tract, which is rich in cardiomyocytes, the BA is mainly composed of smooth muscle [96]. In the *sqet31Et* transgenic line, the BA-associated GFP expression was observed at 72 hpf (Fig. 7A). Accordingly, we observed the enrichment of transcripts encoding several smooth muscle markers, including smooth muscle light chain kinase *mylka*, in the 72 hpf dataset (Fig. 7B). The BA dampens blood pressure fluctuations occurring during different phases of the cardiac cycle [97]. The gene encoding Elnb, which is known to promote the differentiation of smooth muscle cells [53], is expressed in the BA starting from 72 hpf (Fig. 7B). In agreement with this, we found that *elnb* and its paralog *elna* were among genes enriched at 72 hpf compared to 48 hpf. Moreover, we also found the enrichment of other genes previously implicated in maturation and function of elastin, including *ltbp3* and *fbln5* (Fig.7B) [53,98,99]. To date, only one study reported the transcriptome profile of the BA in the adult zebrafish [100]. We found that 56 out of the 59 BA-expressed genes identified in their study were enriched in GFP+ cells at 72 hpf (S15 Table). Taken together,

our results suggest that the 72 hpf transcriptome of GFP+ cells defines genes expressed in the AVC and BA. Nevertheless, the distinctive tissue composition of the BA compared to AVC myocardium allows for segregation based on this criterion. The expression of EGFP in the AVC and BA of *sqet31Et* transgenic line adds to a list of common markers of these cell lineages.

Discussion

The AVC plays two major roles. First, it is part of the CCS which serves as the site where the propagation of electrical impulses is delayed, allowing consecutive contraction of the atrium and ventricle. In mammals, this function is performed by the AV node. Second, the AVC is also the site where the heart valve develops, involving various signaling pathways and cellular rearrangements occurring between different tissue layers. The study of the AVC has been challenging due to the lack of specific molecular markers defining this region. Available data relied on methods based on histological sections [101], which lacks the ability to isolate specific cell types. Nevertheless, it is known that distinct structures of the AVC, such as the pacemaker cells and cardiac valve tissue, express unique combinations of marker genes which can be used to distinguish them.

The transgenic line *sqet31Et* provides the necessary level of specificity, which allows the enrichment of AVC myocardial cells by FACS. By this strategy, in combination with transcriptome analyses, we demonstrate that the zebrafish AVC myocardium possesses hallmarks of the mammalian AV node. The AVC transcriptome is characterized by high expression of mRNA encoding low conductance connexins *cx36.7* and *cx43.4*, as well as the T-type calcium channel *cacna1g* and pacemaker hyperpolarization-activated channel *hcn4*. All these factors are known to define the AV node and pacemaker activity in the mammalian heart [61,72,81,82,102]. The conserved features also extend to the expression of transcripts

encoding the core pacemaker transcriptional network consisting of Tbx2a/2b/3/18 and Shox2 transcription factors.

Previously, the existence of the CCS in zebrafish has been supported by optogenetic studies [27,29] with other evidence suggesting that the endocardium and hemodynamic stimulation play an important role in its development [51,58,103]. The primary SA pacemaker has been relatively better characterized, and it has been shown that its activity depends on Isl1 [21]. Using the *sqet33mi59BEt* transgenic line, we show that the loss of Isl1 in mutants abolishes the SAR, which harbors the primary pacemaker activity. Furthermore, analysis of electrical conduction patterns in *isl1* morphants revealed that, despite being disorganized, atrial activation wave generally still progresses from the SA to AV. This suggests that Isl1 is not the determinant of primary pacemaker function but rather acts in coordinating atrial activation. However, we cannot rule out the possibility that the *isl1* knockdown did not abolish Isl1 function completely. In either case, the lack of an organized atrial activation pattern affects overall cardiac contraction, indicating that the coordinated signaling from the SAR and its propagation play a crucial role in coordinating heart contraction.

Interestingly, during the pause in heart rhythm in Isl1-deficient embryos, the observed increase in AVC activation demonstrated that it possesses inherent automaticity, enabling it to independently excite when a weakened signal from the primary SAR pacemaker is not sufficient to drive heart contractions. This corroborates previous observations in adult zebrafish heart of spontaneous electrical activity at the AV region following surgical uncoupling of the ventricle from the atrium [27]. Comparison of the transcriptome profiles of the SAR and AVC, while revealing common markers of pacemaker activity such as *cacna1g* and *cx43.4*, also indicated differences that would affect electrical properties, such as the enrichment of distinct types of ion channel, gap junction, and extracellular matrix components. This further

supports the notion that, despite their shared ability to act as a pacemaker, the SAR and AVC performs different inherent functions.

The mammalian AV node consists not only of definitive pacemaker cells, but also fibroblasts, macrophages, and ECM, which provide electrical insulation around the electrically conducting AV node, which forms the only point of continuity between cardiac chambers [2,42]. Electrical impulses from the AV node are further propagated by means of an intricate network of His/Purkinje fibers, which link to the thick myocardial tissue throughout the whole ventricle [43]. In contrast, the 2-chambered heart in most fishes resembles the mammalian embryonic heart tube, where electrical current is propagated from one end to the other by means of electrical coupling of cardiomyocytes without a specialized CCS [2]. In fact, the hearts of ectothermic animals do not possess any insulating fibrous structure, although the slow conducting muscles of the AVC is present [20]. Moreover, teleost hearts are not known to possess any defined Purkinje fiber network, and conduction function is served by the ventricular trabeculae, which form myocardial continuity between AVC and apex of the ventricle [104]. Therefore, it is reasonable to assume that conduction function could be served by an equally simplified structure, in which a subset of cardiomyocytes performs pacemaking function and at the same time express additional attributes, which enable it to slow down electrical propagation. Intriguingly, in an earlier analysis of the CCS transgenic lines [51], it was observed in the embryonic heart that cells of the SAR send processes into the AVC, which appeared as a network connecting the two structures. It is therefore tempting to speculate that perhaps a previously uncharacterized structure or cell type may exist in the zebrafish, which facilitates fast conduction between the SAR and AVC.

Besides serving as part of the CCS, the AVC is also the site where the heart valves and septa develop. This process involves several signaling pathways and cellular rearrangements occurring in different tissue layers. We found that the AVC was enriched for transcripts

encoding regulators of EMT, which is a hallmark of endocardial cushion and valve development. Notable examples include *postnb*, which is one of the most highly enriched EMT-related genes at both developmental stages. Its paralog, *postna*, was also enriched in 48 hpf. In mammals, Postn is known to be expressed in the developing endocardial cushion, where an active EMT process is ongoing, but not in cardiomyocytes [105]. Postn acts as an adhesion molecule marking mesenchymal cells in the developing AV valve leaflets [106]. The higher expression of *postna* and *postnb* in GFP+ cells therefore suggests the presence of mesenchymal cells of the valve within this population and suggest an overall heterogeneity of AVC cell populations marked by EGFP expression in the *sqet31Et* transgenic line. Furthermore, components of major signaling pathways, including Wnt, Notch, and TGF-β, which were implicated in endocardial cushion and valve development [33,34], were differentially expressed at 48 to 72 hpf. Canonical Wnt signaling is known to play multiple roles in valve development, including regulation of AVC maturation and establishment of its electrical properties upstream of Tbx3 [89]. We observed that Wnt signaling activity is present not only in AVC endocardial cells, but also in the myocardium. This is in line with the observation in mammalian heart that Wnt ligands originating from the endocardium act as a paracrine signal towards the myocardium, which in turn induces endocardial EMT [34]. In the adult zebrafish heart, a compact group of HCN4-positive cells is embedded within the musculature of the AV valves [27]. The close association between the valve tissues and pacemaker cells is reflected in our transcriptome and adds to the heterogeneity of cell types present within this region. Currently, the bulk RNA-seq approach utilized here does not allow us to distinguish between the various cell populations, nor to clearly demarcate the concurrent developmental processes within the AVC region. Further studies at the single-cell level in both embryonic and adult zebrafish hearts are needed to reveal the true cellular diversity of this structure and more accurately characterize the organization of the CCS in zebrafish heart.

Besides the AVC, the zebrafish *sqet31Et* transgenic line expresses EGFP in the bulbus arteriosus. This expression pattern is driven by the activity of a yet unknown enhancer [50]. The co-expression of EGFP in the BA and cell populations within the AVC region suggests a unifying regulatory principle governing the specification of different cell types present at different spatiotemporal contexts. Some regulatory TFs (Tbx3) are expressed in the AV node and the mesenchyme of the outflow tract, suggesting a similarity of the developmental mechanism in these cell lineages [107]. This poses an interesting question on gene regulation by the regulatory element(s) driving this expression pattern in the sqet31Et transgenic line. For now, it is challenging to identify this enhancer due to the insertion of the enhancer trap construct in genomic repeat regions. However, with the increasing availability of long read sequencing methods, it may be possible in the near future to map the insertion site and trace the identity of this enhancer.

Collectively, our results establish that the zebrafish AVC possesses molecular and physiological hallmarks of a secondary pacemaker, similar to that of the mammalian AV node, in terms of automaticity, low conductance properties, and conserved expression of developmental genes. The partially overlapping expression profiles of genes encoding ion channels and connexins likely underlies the distinct conduction functions between the SAR and AVC. In addition, the dynamic expression of signaling pathways implicated in the ongoing valve development illustrates the role of the AVC in both electrophysiological as well as structural separation between the heart chambers. The AVC transcriptome data generated in this study will enrich our knowledge of molecular factors, as well as identify potential new candidates, implicated in cardiac conduction and valve development.

Methods

Zebrafish

Wild-type, *sqet31Et* and *sqet33mi59BEt* enhancer trap [50,51], and other zebrafish lines used in this study: *Tg(myl7:mRFP)* [108], Wnt reporter line *Tg(7xTCF-Xla.Siam:nlsmCherry)* [88], were maintained in the zebrafish facility of the International Institute of Molecular and Cell Biology in Warsaw (license no. PL14656251) in line with standard procedures and ethical guidelines. *Tg(myl7:mermaid)* was generated by injection of a *Tol2-myl7-mermaid* construct (kind gift of Yasushi Okamura), together with transposase RNA, into 1-2 cell stage AB zebrafish embryos followed by screening for fluorescence progeny. The *isl1* K88X mutant (*isl1*^{sa29}), and *Tg(myl7:mermaid)* was bred and maintained at the Harefield Heart Science Centre according to the Animals (Scientific Procedures) Act 1986. Embryos were raised in egg water at 28°C, screened for a fluorescence signal in the heart and staged at 48 hpf and 72 hpf based on established morphological criteria[109].

Heart extraction and fluorescence-activated cell sorting (FACS)

To isolate the heart, embryos were anesthetized with Tricaine (0.16 mg/ml in egg water) and large-scale extraction was performed according to a previously published protocol, with minor adjustments [110]. GFP-expressing hearts were manually separated from remaining tissue under a fluorescence stereomicroscope and collected into 0,5 ml of EDM (L-15/10% FBS). Pools of 300-500 hearts were dissociated with Trypsin-EDTA solution (0.05%) as previously described [111]. A FACS Aria II cytometer (BD Biosciences, USA) was used to enrich GFP positive (fluorescent) and GFP negative (nonfluorescent) heart fractions. Gates for cell sorting were calibrated against dissociated hearts extracted from wild type zebrafish embryos at the respective developmental stages (48 hpf or 72 hpf). On average, FACS yielded 15-25% of GFP+ events of total singlet events (Supplementary Figure 1A).

RNA extraction

To obtain high-quality total RNA, cells were sorted directly to 500 µl TRIzol™ LS Reagent (Thermo Fisher Scientific, USA) followed by RNA purification and DNase I treatment by means of a Direct-zol™ kit (Zymo Research, USA) according to the manufacturer's protocol. The Tapestation 2200 and High Sensitivity RNA ScreenTape assay (Agilent Technologies, USA) together with Quantus™ Fluorometer (Promega, USA) were used to assess quantity and quality of total RNA. The average RNA Integrity Number equivalent (RIN^e) for samples used for downstream analysis was 8.7.

Library preparation and sequencing

To obtain sequencing libraries, a two-step approach was applied. First, cDNA carrying full-length transcript information was synthesized with SMART-Seq® v4 Ultra® Low Input RNA Kit for Sequencing (TaKaRa Bio, Japan) followed by Nextera XT DNA Library Preparation Kit (Illumina, USA) according to the manufacturer's guidelines. As previously, Tapestation 2200 and dedicated High Sensitivity D5000 ScreenTape and High Sensitivity D1000 ScreenTape assays were used to validate final cDNA and sequencing libraries, respectively. Final libraries were quantified with KAPA Library Quantification Kit Illumina® Platforms (Kapa Biosystems, USA), followed by paired-end sequencing (2 x 75 bp) performed with Nextseq 500 (Illumina, USA). Libraries were sequenced in triplicate, where a single replicate consisted of GFP-positive and GFP-negative fractions for both developmental stages (48 hpf and 72 hpf), at an average depth of 47 million reads.

Analysis of sequencing data

FastQC tool v. 0.11.8 [112] was used to assess the quality of obtained raw RNA-seq reads. Minor adapters contaminations were removed by Cutadapt v. 1.17 [113] and RNA-seq reads were mapped to the zebrafish reference genome (GRCz11) using Salmon tool v. 0.9.1 [37] resulting in an average of 75% mappability rate (S1 Figure C). Sequencing reads were further

631 analyzed in R programming language v. 3.5.2 [114], whereas differentially expressed genes
632 were identified by the DESeq2 package [115]. Principal component analysis was performed on
633 normalized reads counts transformed to the log2 scale by *plotPCA* function from the same
634 package. ClusterProfiler v. 3.17.3 [116] was used to calculate the enrichment of both biological
635 processes of Gene Ontology terms as well as KEGG pathways. The *enrichGO* and *enrichKEGG*
636 functions were used with default *pvalueCutoff* and *qvalueCutoff* parameters. The ggplot2
637 package [117] was utilized for plots generation. All sequencing data have been deposited in the
638 GEO database under accession number GSE160107.

639 **Confocal imaging**

640 Embryos used for imaging were grown in egg water supplemented with 0.003% 1-phenyl 2-
641 thiourea (PTU) at 24 hpf to prevent the formation of melanophores and pigmentation. Prior to
642 imaging, embryos were anesthetized with 0.02% tricaine (MS-222; Sigma-Aldrich A5040),
643 embedded in 1 % low-melt agarose (Sigma, USA) in egg water, and mounted in a glass-bottom
644 dish before imaging on an inverted confocal microscope (LSM800, Zeiss). Images were further
645 processed with Imaris 8 software (Bitplane).

646 **Optical mapping of atrial excitation**

647 To visualize excitation in the embryonic heart, a transgenic zebrafish line expressing the FRET-
648 based voltage-sensitive fluorescent protein Mermaid [118] specifically in myocardial cells
649 *Tg(myl7:mermaid)* was used and optical mapping was performed as described previously, with
650 minor adjustments [119]. Injection of morpholino against *isl1* (5′-
651 TTAATCTGCGTTACCTGATGTAGTC-3′) was performed as previously described [71].
652 Embryos were embedded in 1% low melting agarose on a 35 mm petri dish and oriented ventral
653 side up to the imaging plane. Embedded embryos were transferred to an imaging chamber (RC-
654 29; Harvard Instruments, USA) with a heated platform (PH-6D; Harvard Instruments).

Temperature was maintained at 28°C by a temperature controller (TC-344B; Harvard Instruments). Images were obtained using an epifluorescence upright microscope (BX51WI; Olympus) and focusing module (BXFM; Olympus) with a 40X water immersion objective (LUMPLFLN 40XW; Olympus) and magnification changer (U-CA; Olympus). Fluorescence was excited using a blue light-emitting diode (CBT-90; Luminus, USA) passed through a 460±5 nm bandpass filter (HQ460/10X; Chroma, USA). Fluorescence was collected with a 482 nm dichroic mirror (FF482-Di01; Semrock, USA). To obtain simultaneous images of FRET donor and acceptor signals, collected light was passed into an image splitter (OptoSplit II; Cairn Research, USA), split with a 552 nm dichroic mirror (FF552-Di02; Semrock), and passed through either a 500±30 nm (HQ500/60m-2p; Chroma) or 600±37.5 nm (HQ600/75m; Chroma) bandpass filter. Filtered emission was projected to two halves of a 16-bit, 128×128, 24 mm^2 pixels, cooled electron multiplying charge-coupled device camera (Cascade: 128+; Photometrics, USA) and collected at 52Hz with a ~19 ms exposure time. Images were processed and analyzed using custom routines in MATLAB (R2011b; MathWorks, USA). The ratio of FRET donor and acceptor signals was taken and spatially filtered using the pixelwise adaptive, linear, noise-removal Wiener method ('wiener2') with a 3×3 pixel window. The atrium was manually segmented and each pixel signal normalized through time. Activation time was measured as the point at which the rate of voltage upstroke was maximal.

Electrophysiology

Micropipettes for electrocardiograph (ECG) measurement on whole zebrafish larvae were prepared by pulling fire-polished borosilicate glass capillaries (World Precision Instruments) using the Flaming/brown micropipette puller P-1000 (Sutter Instrument). The zebrafish larvae were mounted (laterally) in 1% low melting agarose in a glass dish and submerged in external buffer: 1x egg water (0.6g/L sea salt in reverse osmosis purified water). The micropipette was filled with internal buffer (174mM NaCl, 2.1mM KCL, 1.2mM MgSO4.7H20, 1.8mM

Ca(NO3)2.4H2O, 15mM HEPES, pH 7.2) and the tip was positioned right above the pericardial region of the zebrafish heart. The electrical signals from the zebrafish heart received were recorded by pCLAMP 10 software (Molecular Devices) after amplification via Multiclamp 700B amplifier (Molecular Devices) and digitization through Axon Digidata 1440A digitizer (Molecular Devices). Data were analysed with Clampfit 10 software (Molecular Devices).

Whole mount *in situ* hybridization

For antisense probes generation, total RNA from 72 hpf embryos was extracted and reverse transcribed into cDNA with SuperScript IV Reverse Transcriptase (Thermo Fisher Scientific, USA). Obtained cDNA was used as a template for PCR. Purified PCR products were used as a template for *in vitro* transcription from the T7 promoter. Primers used are listed in S1 Table or reported previously [51]. Whole mount *in situ* hybridization (WISH) was performed as previously described, with minor adjustments [120]. Zebrafish embryos were grown in egg water containing PTU and fixed overnight at desired developmental stage in 4% paraformaldehyde in 1x PBS (PFA/PBS). After sequential washes with 1x PBT (50 ml 1x PBS + 250 µl 20% Tween-20), embryos were digested for either 30 min (48 hpf) or 50 min (72 hpf) with 10 µg/ml proteinase K (Roche), washed with 1x PBT, and fixed again for 1 hour. PFA/PBS solution was discarded, and embryos were pre-hybridized overnight at 68°C in a hybridization buffer. Subsequently, diluted and denatured probes were added to the pre-hybridized embryos followed by overnight incubation (68°C) in a water bath. Post-hybridization washes were performed in increasing concentration of 2xSSC in the hybridization buffer. To reduce nonspecific signal, commercial blocking reagent (Roche) was used. Signal was visualized by overnight incubation with 1:5000 anti-DIG-AP antibody (Roche) at 4°C followed by washing and addition of NBT and BCIP staining solution. After the staining was fully developed, staining solution was washed away and embryos were fixed in 4% PFA in 1x PBS. For whole mount *in situ* imaging, embryos were mounted in glycerol and imaged on Nikon SMZ25

705 microscope. For each probe, WISH experiments were performed on at least 20 embryos
706 obtained from at least 3 different breeding pairs.

707 Acknowledgements

708 We are grateful to the zebrafish core facility of the IIMCB Warsaw for excellent fish care.
709 We thank Dr. Y. Okamura for the Tol2-*myl7:mermaid* construct and Dr. Natascia Tiso
710 for kindly sharing the *Tg(7x TCF-Xla.Sia:NLS-mCherry)* transgenic line. We thank W. Rybski
711 and Y. Siddiqui for technical help, Drs. D. Stainier, T. Braun, L. Solnica-Krezel, R. Minhas
712 for providing critical advice and fruitful discussions.

713 Competing interests

714 The authors declare that they have no competing interests.

715 References:

716 1. Gourdie RG, Kubalak S, Mikawa T. Conducting the embryonic heart: orchestrating
717 development of specialized cardiac tissues. Trends Cardiovasc. Med. 1999;9:18–26.
718 2. Moorman AFM, Christoffels VM. Development of the cardiac conduction system: a
719 matter of chamber development. Novartis Found. Symp. 2003;250:25–34; discussion 34-
720 43, 276–9.
721 3. Kurian T, Ambrosi C, Hucker W, Fedorov VV, Efimov IR. Anatomy and
722 electrophysiology of the human AV node. Pacing Clin. Electrophysiol. PACE
723 2010;33:754–62.
724 4. Jane B. Reece NAC. Biology, 6th Edition (9780805366242): Reece, Jane B., Campbell,
725 Neil A.: Books. 2002.

5. Wessels A, Markman MW, Vermeulen JL, Anderson RH, Moorman AF, Lamers WH. The development of the atrioventricular junction in the human heart. Circ. Res. 1996;78:110–7.
6. Hucker WJ, Fedorov VV, Foyil KV, Moazami N, Efimov IR. Images in cardiovascular medicine. Optical mapping of the human atrioventricular junction. Circulation 2008;117:1474–7.
7. Heaton J, Yandrapalli S. Premature Atrial Contractions [Internet]. In: StatPearls. Treasure Island (FL): StatPearls Publishing; 2020 [cited 2021 Jan 7]. Available from: http://www.ncbi.nlm.nih.gov/books/NBK559204/
8. Aanhaanen Wim T.J., Brons Janynke F., Domínguez Jorge N., Rana M. Sameer, Norden Julia, Airik Rannar, et al. The Tbx2+ Primary Myocardium of the Atrioventricular Canal Forms the Atrioventricular Node and the Base of the Left Ventricle. Circ. Res. 2009;104:1267–74.
9. Christoffels VM, Hoogaars WMH, Tessari A, Clout DEW, Moorman AFM, Campione M. T-box transcription factor Tbx2 represses differentiation and formation of the cardiac chambers. Dev. Dyn. Off. Publ. Am. Assoc. Anat. 2004;229:763–70.
10. Singh R, Hoogaars WM, Barnett P, Grieskamp T, Rana MS, Buermans H, et al. Tbx2 and Tbx3 induce atrioventricular myocardial development and endocardial cushion formation. Cell. Mol. Life Sci. CMLS 2012;69:1377–89.
11. Boyett MR, Inada S, Yoo S, Li J, Liu J, Tellez J, et al. Connexins in the sinoatrial and atrioventricular nodes. Adv. Cardiol. 2006;42:175–97.
12. Dobrzynski H, Anderson RH, Atkinson A, Borbas Z, D'Souza A, Fraser JF, et al. Structure, function and clinical relevance of the cardiac conduction system, including the atrioventricular ring and outflow tract tissues. Pharmacol. Ther. 2013;139:260–88.

13. Coppen SR, Gourdie RG, Severs NJ. Connexin45 is the first connexin to be expressed in the central conduction system of the mouse heart. Exp. Clin. Cardiol. 2001;6:17–23.
14. Kreuzberg MM, Willecke K, Bukauskas FF. Connexin-Mediated Cardiac Impulse Propagation: Connexin 30.2 Slows Atrioventricular Conduction in Mouse Heart. Trends Cardiovasc. Med. 2006;16:266–72.
15. Moreno AP, Sáez JC, Fishman GI, Spray DC. Human connexin43 gap junction channels. Regulation of unitary conductances by phosphorylation. Circ. Res. 1994;74:1050–7.
16. Veenstra RD. Do connexin channels have a residual conductance state? Biophys. J. 1996;70:1082–4.
17. Gemel J, Lin X, Collins R, Veenstra RD, Beyer EC. Cx30.2 can form heteromeric gap junction channels with other cardiac connexins. Biochem. Biophys. Res. Commun. 2008;369:388–94.
18. Chi NC, Shaw RM, Jungblut B, Huisken J, Ferrer T, Arnaout R, et al. Genetic and Physiologic Dissection of the Vertebrate Cardiac Conduction System. PLOS Biol. 2008;6:e109.
19. Milan DJ, Jones IL, Ellinor PT, MacRae CA. In vivo recording of adult zebrafish electrocardiogram and assessment of drug-induced QT prolongation. Am. J. Physiol. Heart Circ. Physiol. 2006;291:H269-273.
20. Jensen B, Boukens BJD, Postma AV, Gunst QD, Hoff MJB van den, Moorman AFM, et al. Identifying the Evolutionary Building Blocks of the Cardiac Conduction System. PLOS ONE 2012;7:e44231.
21. Tessadori F, van Weerd JH, Burkhard SB, Verkerk AO, de Pater E, Boukens BJ, et al. Identification and functional characterization of cardiac pacemaker cells in zebrafish. PloS One 2012;7:e47644.

774 22. Karlsson O, Thor S, Norberg T, Ohlsson H, Edlund T. Insulin gene enhancer binding
775 protein Isl-1 is a member of a novel class of proteins containing both a homeo- and a Cys-
776 His domain. Nature 1990;344:879–82.
777 23. Korzh V, Edlund T, Thor S. Zebrafish primary neurons initiate expression of the LIM
778 homeodomain protein Isl-1 at the end of gastrulation. Dev. Camb. Engl. 1993;118:417–
779 25.
780 24. Inoue A, Takahashi M, Hatta K, Hotta Y, Okamoto H. Developmental regulation of islet-
781 1 mRNA expression during neuronal differentiation in embryonic zebrafish. Dev. Dyn.
782 Off. Publ. Am. Assoc. Anat. 1994;199:1–11.
783 25. de Pater E, Clijsters L, Marques SR, Lin Y-F, Garavito-Aguilar ZV, Yelon D, et al.
784 Distinct phases of cardiomyocyte differentiation regulate growth of the zebrafish heart.
785 Dev. Camb. Engl. 2009;136:1633–41.
786 26. Stoyek MR, Croll RP, Smith FM. Intrinsic and extrinsic innervation of the heart in
787 zebrafish (Danio rerio). J. Comp. Neurol. 2015;523:1683–700.
788 27. Stoyek MR, Quinn TA, Croll RP, Smith FM. Zebrafish heart as a model to study the
789 integrative autonomic control of pacemaker function. Am. J. Physiol. Heart Circ. Physiol.
790 2016;311:H676-688.
791 28. Colombo S, de Sena-Tomás C, George V, Werdich AA, Kapur S, MacRae CA, et al. Nkx
792 genes establish second heart field cardiomyocyte progenitors at the arterial pole and
793 pattern the venous pole through Isl1 repression. Dev. Camb. Engl. [Internet] 2018 [cited
794 2021 Jan 7];145. Available from:
795 https://www.ncbi.nlm.nih.gov/pmc/articles/PMC5818010/
796 29. Arrenberg AB, Stainier DYR, Baier H, Huisken J. Optogenetic control of cardiac
797 function. Science 2010;330:971–4.

30. Peal DS, Lynch SN, Milan DJ. Patterning and Development of the Atrioventricular Canal in Zebrafish. J Cardiovasc. Transl. Res. 2011;4:720–6.
31. Lamouille S, Xu J, Derynck R. Molecular mechanisms of epithelial–mesenchymal transition. Nat. Rev. Mol. Cell Biol. 2014;15:178–96.
32. Schroeder JA, Jackson LF, Lee DC, Camenisch TD. Form and function of developing heart valves: coordination by extracellular matrix and growth factor signaling. J. Mol. Med. Berl. Ger. 2003;81:392–403.
33. Garside VC, Chang AC, Karsan A, Hoodless PA. Co-ordinating Notch, BMP, and TGF-β signaling during heart valve development. Cell. Mol. Life Sci. CMLS 2013;70:2899–917.
34. Wang Y, Wu B, Chamberlain AA, Lui W, Koirala P, Susztak K, et al. Endocardial to myocardial notch-wnt-bmp axis regulates early heart valve development. PloS One 2013;8:e60244.
35. Beis D, Bartman T, Jin S-W, Scott IC, D'Amico LA, Ober EA, et al. Genetic and cellular analyses of zebrafish atrioventricular cushion and valve development. Dev. Camb. Engl. 2005;132:4193–204.
36. Walsh EC, Stainier DY. UDP-glucose dehydrogenase required for cardiac valve formation in zebrafish. Science 2001;293:1670–3.
37. Patro R, Duggal G, Love MI, Irizarry RA, Kingsford C. Salmon provides fast and bias-aware quantification of transcript expression. Nat. Methods 2017;14:417–9.
38. Hurlstone AFL, Haramis A-PG, Wienholds E, Begthel H, Korving J, Van Eeden F, et al. The Wnt/beta-catenin pathway regulates cardiac valve formation. Nature 2003;425:633–7.
39. Martin RT, Bartman T. Analysis of heart valve development in larval zebrafish. Dev. Dyn. Off. Publ. Am. Assoc. Anat. 2009;238:1796–802.

822 40. Verhoeven MC, Haase C, Christoffels VM, Weidinger G, Bakkers J. Wnt signaling
823 regulates atrioventricular canal formation upstream of BMP and Tbx2. Birt. Defects Res.
824 A. Clin. Mol. Teratol. 2011;91:435–40.
825 41. Milan DJ, Giokas AC, Serluca FC, Peterson RT, MacRae CA. Notch1b and neuregulin
826 are required for specification of central cardiac conduction tissue. Development
827 2006;133:1125–32.
828 42. Lockhart MM, Phelps AL, van den Hoff MJB, Wessels A. The Epicardium and the
829 Development of the Atrioventricular Junction in the Murine Heart. J. Dev. Biol.
830 2014;2:1–17.
831 43. Anderson RH, Yanni J, Boyett MR, Chandler NJ, Dobrzynski H. The anatomy of the
832 cardiac conduction system. Clin. Anat. N. Y. N 2009;22:99–113.
833 44. Poon KL, Brand T. The zebrafish model system in cardiovascular research: A tiny fish
834 with mighty prospects. Glob. Cardiol. Sci. Pract. 2013;2013:9–28.
835 45. Stoyek MR, Quinn TA. One fish, two fish, red fish, blue fish*: Zebrafish as a model for
836 cardiac research. Prog. Biophys. Mol. Biol. 2018;138:1–2.
837 46. Ebert AM, Hume GL, Warren KS, Cook NP, Burns CG, Mohideen MA, et al. Calcium
838 extrusion is critical for cardiac morphogenesis and rhythm in embryonic zebrafish hearts.
839 Proc. Natl. Acad. Sci. U. S. A. 2005;102:17705–10.
840 47. Arnaout R, Ferrer T, Huisken J, Spitzer K, Stainier DYR, Tristani-Firouzi M, et al.
841 Zebrafish model for human long QT syndrome. Proc. Natl. Acad. Sci. U. S. A.
842 2007;104:11316–21.
843 48. Hassel David, Scholz Eberhard P., Trano Nicole, Friedrich Oliver, Just Steffen, Meder
844 Benjamin, et al. Deficient Zebrafish Ether-à-Go-Go–Related Gene Channel Gating
845 Causes Short-QT Syndrome in Zebrafish Reggae Mutants. Circulation 2008;117:866–75.

846 49. Huttner IG, Trivedi G, Jacoby A, Mann SA, Vandenberg JI, Fatkin D. A transgenic
847 zebrafish model of a human cardiac sodium channel mutation exhibits bradycardia,
848 conduction-system abnormalities and early death. J. Mol. Cell. Cardiol. 2013;61:123–32.
849 50. Poon K-L, Liebling M, Kondrychyn I, Garcia-Lecea M, Korzh V. Zebrafish cardiac
850 enhancer trap lines: new tools for in vivo studies of cardiovascular development and
851 disease. Dev. Dyn. Off. Publ. Am. Assoc. Anat. 2010;239:914–26.
852 51. Poon K-L, Liebling M, Kondrychyn I, Brand T, Korzh V. Development of the cardiac
853 conduction system in zebrafish. Gene Expr. Patterns GEP 2016;21:89–96.
854 52. Minhas R, Löffler-Wirth H, Siddiqui Y, Obrebski T, Vhashist S, Aby Nahia K, et al.
855 Transcriptome Profile of the Sinoatrial Ring Reveals Conserved and Novel Genetic
856 Programs of the Zebrafish Pacemaker. 2020. Research Square [Preprint]. December 21,
857 2020 [cited 2021 Jan 15]. Available from: https://doi.org/10.21203/rs.3.rs-130687/v1.
858 53. Moriyama Y, Ito F, Takeda H, Yano T, Okabe M, Kuraku S, et al. Evolution of the fish
859 heart by sub/neofunctionalization of an elastin gene. Nat. Commun. 2016;7:10397.
860 54. Smith C, Hayamizu T, Finger J, Bello S, McCright I, Xu J, et al. The mouse Gene
861 Expression Database (GXD): 2019 update. Nucleic Acids Res. 2018;47.
862 55. Nguyen CT, Langenbacher A, Hsieh M, Chen J-N. The PAF1 complex component Leo1
863 is essential for cardiac and neural crest development in zebrafish. Dev. Biol.
864 2010;341:167–75.
865 56. Lee H-C, Lo H-C, Lo D-M, Su M-Y, Hu J-R, Wu C-C, et al. Amiodarone Induces
866 Overexpression of Similar to Versican b to Repress the EGFR/Gsk3b/Snail Signaling
867 Axis during Cardiac Valve Formation of Zebrafish Embryos. PLOS ONE
868 2015;10:e0144751.

869 57. Jia H, King IN, Chopra SS, Wan H, Ni TT, Jiang C, et al. Vertebrate heart growth is
870 regulated by functional antagonism between Gridlock and Gata5. Proc. Natl. Acad. Sci.
871 U. S. A. 2007;104:14008–13.
872 58. Ahuja S, Dogra D, Stainier DYR, Reischauer S. Id4 functions downstream of Bmp
873 signaling to restrict TCF function in endocardial cells during atrioventricular valve
874 development. Dev. Biol. 2016;412:71–82.
875 59. Sultana N, Nag K, Hoshijima K, Laird DW, Kawakami A, Hirose S. Zebrafish early
876 cardiac connexin, Cx36.7/Ecx, regulates myofibril orientation and heart morphogenesis
877 by establishing Nkx2.5 expression. Proc. Natl. Acad. Sci. 2008;105:4763–8.
878 60. Watanabe M. Gap Junction in the Teleost Fish Lineage: Duplicated Connexins May
879 Contribute to Skin Pattern Formation and Body Shape Determination. Front. Cell Dev.
880 Biol. 2017;5:13.
881 61. Frank Marina, Wirth Angela, Andrié René P., Kreuzberg Maria M., Dobrowolski
882 Radoslaw, Seifert Gerald, et al. Connexin45 Provides Optimal Atrioventricular Nodal
883 Conduction in the Adult Mouse Heart. Circ. Res. 2012;111:1528–38.
884 62. Chi NC, Bussen M, Brand-Arzamendi K, Ding C, Olgin JE, Shaw RM, et al. Cardiac
885 conduction is required to preserve cardiac chamber morphology. Proc. Natl. Acad. Sci. U.
886 S. A. 2010;107:14662–7.
887 63. Temple IP, Inada S, Dobrzynski H, Boyett MR. Connexins and the atrioventricular node.
888 Heart Rhythm 2013;10:297–304.
889 64. Bakker ML, Moorman AFM, Christoffels VM. The Atrioventricular Node: Origin,
890 Development, and Genetic Program. Trends Cardiovasc. Med. 2010;20:164–71.
891 65. Christoffels VM, Smits GJ, Kispert A, Moorman AFM. Development of the pacemaker
892 tissues of the heart. Circ. Res. 2010;106:240–54.

893 66. Goodyer William R., Beyersdorf Benjamin M., Paik David T., Tian Lei, Li Guang,
894 Buikema Jan W., et al. Transcriptomic Profiling of the Developing Cardiac Conduction
895 System at Single-Cell Resolution. Circ. Res. 2019;125:379–97.
896 67. Hoogaars WMH, Tessari A, Moorman AFM, de Boer PAJ, Hagoort J, Soufan AT, et al.
897 The transcriptional repressor Tbx3 delineates the developing central conduction system of
898 the heart. Cardiovasc. Res. 2004;62:489–99.
899 68. Espinoza-Lewis RA, Yu L, He F, Liu H, Tang R, Shi J, et al. Shox2 is essential for the
900 differentiation of cardiac pacemaker cells by repressing Nkx2-5. Dev. Biol.
901 2009;327:376–85.
902 69. Wiese C, Grieskamp T, Airik R, Mommersteeg MTM, Gardiwal A, de Gier-de Vries C, et
903 al. Formation of the sinus node head and differentiation of sinus node myocardium are
904 independently regulated by Tbx18 and Tbx3. Circ. Res. 2009;104:388–97.
905 70. Aanhaanen WTJ, Moorman AFM, Christoffels VM. Origin and development of the
906 atrioventricular myocardial lineage: insight into the development of accessory pathways.
907 Birt. Defects Res. A. Clin. Mol. Teratol. 2011;91:565–77.
908 71. Hutchinson SA, Eisen JS. Islet1 and Islet2 have equivalent abilities to promote
909 motoneuron formation and to specify motoneuron subtype identity. Dev. Camb. Engl.
910 2006;133:2137–47.
911 72. Mangoni ME, Couette B, Marger L, Bourinet E, Striessnig J, Nargeot J. Voltage-
912 dependent calcium channels and cardiac pacemaker activity: from ionic currents to genes.
913 Prog. Biophys. Mol. Biol. 2006;90:38–63.
914 73. Launay P, Fleig A, Perraud A-L, Scharenberg AM, Penner R, Kinet J-P. TRPM4 Is a
915 Ca2+-Activated Nonselective Cation Channel Mediating Cell Membrane Depolarization.
916 Cell 2002;109:397–407.

74. Kruse M, Schulze-Bahr E, Corfield V, Beckmann A, Stallmeyer B, Kurtbay G, et al. Impaired endocytosis of the ion channel TRPM4 is associated with human progressive familial heart block type I. J. Clin. Invest. 2009;119:2737–44.

75. Coban-Akdemir ZH, Charng W-L, Azamian M, Paine IS, Punetha J, Grochowski CM, et al. Wolff-Parkinson-White syndrome: De novo variants and evidence for mutational burden in genes associated with atrial fibrillation. Am. J. Med. Genet. A. 2020;182:1387–99.

76. Anderson RH, Ho SY. Anatomy of the atrioventricular junctions with regard to ventricular preexcitation. Pacing Clin. Electrophysiol. PACE 1997;20:2072–6.

77. Abbott GW. Regulation of human cardiac potassium channels by full-length KCNE3 and KCNE4. Sci. Rep. 2016;6:38412.

78. Splawski I, Timothy KW, Sharpe LM, Decher N, Kumar P, Bloise R, et al. Ca(V)1.2 calcium channel dysfunction causes a multisystem disorder including arrhythmia and autism. Cell 2004;119:19–31.

79. Arking DE, Pulit SL, Crotti L, van der Harst P, Munroe PB, Koopmann TT, et al. Genetic association study of QT interval highlights role for calcium signaling pathways in myocardial repolarization. Nat. Genet. 2014;46:826–36.

80. Jansen JA, van Veen TAB, de Bakker JMT, van Rijen HVM. Cardiac connexins and impulse propagation. J. Mol. Cell. Cardiol. 2010;48:76–82.

81. Kreuzberg MM, Willecke K, Bukauskas FF. Connexin-mediated cardiac impulse propagation: connexin 30.2 slows atrioventricular conduction in mouse heart. Trends Cardiovasc. Med. 2006;16:266–72.

82. Kreuzberg MM, Schrickel JW, Ghanem A, Kim J-S, Degen J, Janssen-Bienhold U, et al. Connexin30.2 containing gap junction channels decelerate impulse propagation through the atrioventricular node. Proc. Natl. Acad. Sci. U. S. A. 2006;103:5959–64.

942 83. Molin DGM, Bartram U, Van der Heiden K, Van Iperen L, Speer CP, Hierck BP, et al.
943 Expression patterns of Tgfbeta1-3 associate with myocardialisation of the outflow tract
944 and the development of the epicardium and the fibrous heart skeleton. Dev. Dyn. Off.
945 Publ. Am. Assoc. Anat. 2003;227:431–44.
946 84. Timmerman LA, Grego-Bessa J, Raya A, Bertrán E, Pérez-Pomares JM, Díez J, et al.
947 Notch promotes epithelial-mesenchymal transition during cardiac development and
948 oncogenic transformation. Genes Dev. 2004;18:99–115.
949 85. Luna-Zurita L, Prados B, Grego-Bessa J, Luxán G, del Monte G, Benguría A, et al.
950 Integration of a Notch-dependent mesenchymal gene program and Bmp2-driven cell
951 invasiveness regulates murine cardiac valve formation. J. Clin. Invest. 2010;120:3493–
952 507.
953 86. Chen I-H, Wang H-H, Hsieh Y-S, Huang W-C, Yeh H-I, Chuang Y-J. PRSS23 is
954 essential for the Snail-dependent endothelial-to-mesenchymal transition during
955 valvulogenesis in zebrafish. Cardiovasc. Res. 2013;97:443–53.
956 87. Alfieri CM, Cheek J, Chakraborty S, Yutzey KE. Wnt signaling in heart valve
957 development and osteogenic gene induction. Dev. Biol. 2010;338:127.
958 88. Moro E, Ozhan-Kizil G, Mongera A, Beis D, Wierzbicki C, Young RM, et al. In vivo
959 Wnt signaling tracing through a transgenic biosensor fish reveals novel activity domains.
960 Dev. Biol. 2012;366:327–40.
961 89. Gillers BS, Chiplunkar A, Aly H, Valenta T, Basler K, Christoffels VM, et al. Canonical
962 wnt signaling regulates atrioventricular junction programming and electrophysiological
963 properties. Circ. Res. 2015;116:398–406.
964 90. Pick A, Langendorf R, Katz LN. A-V nodal tachycardia with block. Circulation
965 1961;24:12–22.
966 91. Ganz LI, Friedman PL. Supraventricular tachycardia. N. Engl. J. Med. 1995;332:162–73.

967 92. McDermott DA, Bressan MC, He J, Lee JS, Aftimos S, Brueckner M, et al. TBX5 genetic
968 testing validates strict clinical criteria for Holt-Oram syndrome. Pediatr. Res.
969 2005;58:981–6.
970 93. Basson CT, Bachinsky DR, Lin RC, Levi T, Elkins JA, Soults J, et al. Mutations in
971 human TBX5 [corrected] cause limb and cardiac malformation in Holt-Oram syndrome.
972 Nat. Genet. 1997;15:30–5.
973 94. Ching Y-H, Ghosh TK, Cross SJ, Packham EA, Honeyman L, Loughna S, et al. Mutation
974 in myosin heavy chain 6 causes atrial septal defect. Nat. Genet. 2005;37:423–8.
975 95. Holm H, Gudbjartsson DF, Sulem P, Masson G, Helgadottir HT, Zanon C, et al. A rare
976 variant in MYH6 is associated with high risk of sick sinus syndrome. Nat. Genet.
977 2011;43:316–20.
978 96. Braun MH, Brill RW, Gosline JM, Jones DR. Form and function of the bulbus arteriosus
979 in yellowfin tuna (Thunnus albacares): dynamic properties. J. Exp. Biol. 2003;206:3327–
980 35.
981 97. Farrell AP. The Wind-Kessel effect of the bulbus arteriosus in trout. J. Exp. Zool.
982 1979;209:169–73.
983 98. Hirai M, Horiguchi M, Ohbayashi T, Kita T, Chien KR, Nakamura T. Latent TGF-beta-
984 binding protein 2 binds to DANCE/fibulin-5 and regulates elastic fiber assembly. EMBO
985 J. 2007;26:3283–95.
986 99. Noda K, Dabovic B, Takagi K, Inoue T, Horiguchi M, Hirai M, et al. Latent TGF-β
987 binding protein 4 promotes elastic fiber assembly by interacting with fibulin-5. Proc. Natl.
988 Acad. Sci. U. S. A. 2013;110:2852–7.
989 100. Singh AR, Sivadas A, Sabharwal A, Vellarikal SK, Jayarajan R, Verma A, et al.
990 Chamber Specific Gene Expression Landscape of the Zebrafish Heart. PLOS ONE
991 2016;11:e0147823.

992 101. Burkhard SB, Bakkers J. Spatially resolved RNA-sequencing of the embryonic heart
993 identifies a role for Wnt/β-catenin signaling in autonomic control of heart rate. eLife
994 2018;7:e31515.
995 102. Stieber J, Herrmann S, Feil S, Löster J, Feil R, Biel M, et al. The hyperpolarization-
996 activated channel HCN4 is required for the generation of pacemaker action potentials in
997 the embryonic heart. Proc. Natl. Acad. Sci. U. S. A. 2003;100:15235–40.
998 103. Stainier DY, Fouquet B, Chen JN, Warren KS, Weinstein BM, Meiler SE, et al.
999 Mutations affecting the formation and function of the cardiovascular system in the
1000 zebrafish embryo. Dev. Camb. Engl. 1996;123:285–92.
1001 104. Sedmera D, Reckova M, DeAlmeida A, Coppen SR, Kubalak SW, Gourdie RG, et al.
1002 Spatiotemporal pattern of commitment to slowed proliferation in the embryonic mouse
1003 heart indicates progressive differentiation of the cardiac conduction system. Anat. Rec. A.
1004 Discov. Mol. Cell. Evol. Biol. 2003;274:773–7.
1005 105. Kruzynska-Frejtag A, Machnicki M, Rogers R, Markwald RR, Conway SJ. Periostin
1006 (an osteoblast-specific factor) is expressed within the embryonic mouse heart during valve
1007 formation. Mech. Dev. 2001;103:183–8.
1008 106. Snider P, Hinton RB, Moreno-Rodriguez RA, Wang J, Rogers R, Lindsley A, et al.
1009 Periostin is required for maturation and extracellular matrix stabilization of
1010 noncardiomyocyte lineages of the heart. Circ. Res. 2008;102:752–60.
1011 107. Washkowitz AJ, Gavrilov S, Begum S, Papaioannou VE. Diverse functional networks
1012 of Tbx3 in development and disease. Wiley Interdiscip. Rev. Syst. Biol. Med.
1013 2012;4:273–83.
1014 108. Rohr S, Otten C, Abdelilah-Seyfried S. Asymmetric involution of the myocardial field
1015 drives heart tube formation in zebrafish. Circ. Res. 2008;102:e12-19.

109. Kimmel CB, Ballard WW, Kimmel SR, Ullmann B, Schilling TF. Stages of embryonic development of the zebrafish. Dev. Dyn. Off. Publ. Am. Assoc. Anat. 1995;203:253–310.

110. Lombardo VA, Otten C, Abdelilah-Seyfried S. Large-scale zebrafish embryonic heart dissection for transcriptional analysis. J. Vis. Exp. JoVE 2015;52087.

111. Winata CL, Kondrychyn I, Kumar V, Srinivasan KG, Orlov Y, Ravishankar A, et al. Genome Wide Analysis Reveals Zic3 Interaction with Distal Regulatory Elements of Stage Specific Developmental Genes in Zebrafish. PLOS Genet. 2013;9:e1003852.

112. Andrews S, Krueger F, Segonds-Pichon A. FastQC: a quality control tool for high throughput sequence data. Camb. UK Babraham Inst. [Internet] 2011;Available from: Available online at: http://www.bioinformatics.babraham.ac.uk/projects/fastqc.

113. Martin M. Cutadapt removes adapter sequences from high-throughput sequencing reads. EMBnet.journal 2011;17:10–2.

114. R Core Team. R: a language and environment for statistical computing [Internet]. 2019 [cited 2021 Jan 7];Available from: https://www.gbif.org/tool/81287/r-a-language-and-environment-for-statistical-computing

115. Love MI, Huber W, Anders S. Moderated estimation of fold change and dispersion for RNA-seq data with DESeq2. Genome Biol. 2014;15:550.

116. Yu G, Wang L-G, Han Y, He Q-Y. clusterProfiler: an R Package for Comparing Biological Themes Among Gene Clusters. OMICS J. Integr. Biol. 2012;16:284–7.

117. Wickham H. ggplot2: Elegant Graphics for Data Analysis [Internet]. New York: Springer-Verlag; 2009 [cited 2021 Jan 7]. Available from: https://www.springer.com/gp/book/9780387981413

118. Tsutsui H, Karasawa S, Okamura Y, Miyawaki A. Improving membrane voltage measurements using FRET with new fluorescent proteins. Nat. Methods 2008;5:683–5.

119. Tsutsui H, Higashijima S, Miyawaki A, Okamura Y. Visualizing voltage dynamics in zebrafish heart. J. Physiol. 2010;588:2017–21.

120. Thisse C, Thisse B. High-resolution in situ hybridization to whole-mount zebrafish embryos. Nat. Protoc. 2008;3:59–69.

Figure Legend

Figure 1. EGFP expression in the transgenic line sqet31Et defines cells of the AVC. (A, B) confocal images showing the AVC region at 48 hpf and 72 hpf. Note the overlap between EGFP and mRFP signals, indicating extensive co-localization and confirming the largely myocardial nature of the EGFP expression domain in *sqet31Et*. (C, D) Close-up of the region marked in panel B at different focal planes showing the surface (C) and lumen (D) of the AVC. Note the group of 3 cuboidal cells protruding into the cardiac lumen at the location corresponding to the developing cardiac cushion (asterisk). (E, F) Whole-mount *in situ* hybridization of *egfp* in *sqet31Et* transgenic embryos at 72 hpf showing enrichment of EGFP expression in the AVC relative to the rest of the heart. E - ventral, D - lateral view, A - atrium, V - ventricle, AVC - atrioventricular canal, BA - bulbus arteriosus, AVM - atrioventricular myocardium.

Figure 2. Transcriptome profiling of the GFP+ cells isolated from *sqet31Et.* (A) Scheme of experimental design. (B) Principal component analysis (PCA) on normalized RNA-seq data (regularized log) showing variance between three technical replicates of each sample as well as between samples. (C, F) Volcano plots showing genes differentially expressed between EGFP-positive and -negative cells at 48 hpf (C) and 72 hpf (F). DESeq2 was used to calculate log2FC and padj values. Green spots indicate genes considered as significant (padj < 0.05) with at least two-fold change between groups (log2FC > 2). Accordingly, light red spots represent significant genes with log2FC smaller than -2. (D, G) KEGG pathway enrichment of

differentially expressed genes at 48 hpf and 72 hpf. Enrichment analysis was performed on a gene list meeting the following criteria: log2FC >2 or log2FC < -2 and padj < 0.05. Same criteria were used to perform biological process Gene Ontology terms enrichment on up and down-regulated genes (E, H). Top 10 terms for each enrichment analysis were shown.

Figure 3. AVC gene signatures are enriched in *sqet31Et* EGFP-expressing cells. Signatures were retrieved from MGI and ZFIN databases and used to identify molecular markers associated with AVC expressed in the studied dataset (padj < 0.05). (A) Heatmap depicts the dynamic of changes of known molecular AVC signatures that are in common across the developmental stage. (B) AVC markers uniquely expressed in either 48 hpf or 72 hpf stage. (C) Expression (in log10(TPM +1)) of genes encoding connexins, components of gap junctions which confer conductance properties between cells, in GFP+ and GFP- cells at 48 hpf and 72 hpf. Mammalian homologs of each connexin gene and their known conductance properties are described in the accompanying table.

Figure 4. The absence of the pacemaker ring in *isl1* mutant causes the loss of expression of *fhf2, hcn4, bmp4*. (A-H) Expression pattern (labeled with arrow) of *fhf2a* (A, B), *bmp4* (C, D), *hcn4* (E, F) and EGFP (G, H) in *isl1* siblings and mutants. (A- F) - WISH, (G, H) - confocal microscopy of CCS in the sibling and *isl1* mutant. (I) Representative image of CCS transgenics control embryo and *isl1* overexpressed embryos at 40 hpf. (J) The table presents the mean, standard deviation, and minimum and maximum grey value (determined in Image J) as the measured EGFP fluorescence intensity of the pacemaker cells at 40 hpf. The numbers (N) of embryos used for measurement is indicated.

Figure 5. Effects of morpholino knockdown of isl1 on electrical activity of the atria in zebrafish larvae. (A) Heart rate at 48 hpf (left) and 72 hpf (right) in WT control (red) and *isl1* morphant (blue) zebrafish, showing slowed heart rate in *isl1* morphants. *p<0.001.

(C) Videographic analysis of the heartbeat in WT control (top) and *isl1* morphant (bottom) 48 hpf zebrafish, showing slowed heart rate and sinus pauses (during the period indicated by the arrow) in the *isl1* morphant. (B) Sequence of video frames showing electrical activation of the atria in WT control (left) and *isl1* morphant (right) 48 hpf *Tg*(*myl7:mermaid*) zebrafish, showing normal activation (from the sinoatrial node region [SA] to the atrioventricular [AV] junction) and sites of latest activation/repolarisation (indicated by red stars) in the WT control and abnormal activation in the *isl1* morphant (sites of early/ectopic activation in the morphant zebrafish indicated by green stars). (D) Isochronal activation map of the atria in WT control (left) and *isl1* morphant (right) 48 hpf zebrafish derived from the video represented in B.

Figure 6. The transcripts of genes involved in EMT and valve development are enriched in the AVC. (A) AVC-enrichment (expressed in log2 fold change between GFP+ and GFP- cells, padj < 0.05) of genes known to regulate EMT at both 48 hpf and 72 hpf stages. (B) Overlap of EMT-regulating genes enriched in GFP+ cells at both stages. (C-D) Volcano plot showing enrichment of components of the TGF-β and Wnt signaling pathways in AVC at both 48 hpf and 72 hpf stages. (E) Whole mount *in situ* hybridization of several AVC-enriched genes of the TGF-β and Wnt pathway components.

Figure 7. Bulbus arteriosus constitute the 72 hpf transcriptome. (A) Confocal image of the heart in double transgenic line *sqet31Et* x *Tg(myl7*:*mRFP*) at 72 hpf showing additional EGFP expression domain in the bulbus arteriosus (BA). (B) Genes previously known to be expressed in the BA are enriched at 72 hpf compared to 48 hpf. In the zebrafish, the BA is composed of smooth muscle and is rich in elastin and contractile proteins. Note the high enrichment of *elnb* at 72 hpf as compared to 48 hpf.

Supporting information

S1 Figure. Sample quality measures. (A) Analysis of FACS sorting of cardiac cells from the *sqet31Et* transgenic line. Forward scatter (FSC-A) vs side scatter (SSC-A) was used to find viable, single cell events; SSC-A vs GFP-A was applied to identify fluorescent cells. (B) Box plot showing distribution of EGFP transcript levels as a result of BLAST search against EGFP sequence in three different replicates of each sample type. Note the significant enrichment of EGFP expression in EGFP-positive samples as compared to negative, which is reflected by the fold change 52.5 and 75.6 for 48 hpf and 72 hpf, respectively. Mappability of RNA-seq reads in three replicas of each sample type. (C) Box plot of sequencing reads mapping rates in each sample type. Average mapping rate for all the samples was around 75%.

S2 Figure. Expression validation of AVC-enriched genes by whole mount *in situ* hybridization at 72 hpf, except for *smpx* (48 hpf). Images show the frontal view of the embryos. The AVC region is indicated by white arrowheads. BA – bulbus arteriosus.

S3 Figure. Overview of known gene signatures associated with the atrioventricular node and pacemaker in general, expressed as a normalized expression value (regularized log [rld]). Both positive and negative markers (working myocardium) were shown.

S4 Figure. Wnt signaling activity in different layers of the AVC. Double transgenic line *sqet31Et* x *Tg(7xTCFXla.Siam:nlsmCherry)* were generated in order to visualize Wnt signaling activity (represented by mCherry expression) in the AVC region. (A-C) Fluorescent image showing Wnt signaling activity in cells of the endocardial cushion (ECs). (C - H) confocal image of the AVC at the surface (C-E) and lumen (F-H) reveals overlap of mCherry expression with that of EGFP in the *sqet31Et* line, indicating additional Wnt signaling activity in the AV myocardium (AVM).

S5 Figure. Developmental signaling pathway genes with dynamic expression between 72 hpf and 48 hpf. (A) Volcano plot representing the expression of various components of

Notch, TGF-β and Wnt signalling pathways in the AVC myocardium (padj < 0.05, -1 < log2FoldChange > 1). (B) Overrepresented Gene Ontology terms at 72 hpf as compared to 48 hpf.

S1 Table. List of primers for *in situ* probes.

S2 Table. Master list of GFP+ vs - differentially expressed genes at both stages.

S3 Table. GO enrichment analysis of enriched genes at both stages.

S4 Table. Common AVC gene signatures between 48 hpf and 72 hpf.

S5 Table. Connexins enriched in the GFP+ population at both developmental stages.

S6 Table. Genes associated with atrioventricular node or pacemaker development and function.

S7 Table. AVC and SAR intersection.

S8 Table. Genes involved in the EMT process enriched in the GFP+ compared to GFP- cell population.

S9 Table. Master list of GFP+ differentially expressed genes between 72 hpf vs 48 hpf.

S10 Table. GO analysis of differentially expressed genes at 72 hpf vs 48 hpf.

S11 Table. List of significant gene members of three signaling pathways.

S12 Table. Results of ClinVar search database in terms of GWAS study related to the cardiac conduction system.

S13 Table. Results of ClinVar search database in terms of GWAS study related to the valve.

1156 **S14 Table. Results of ClinVar search database in terms of GWAS study related to the**

1157 **heart septal defects.**

1158 **S15 Table. Bulbus arteriosus genes enriched in GFP+ cells at 72 hpf.**

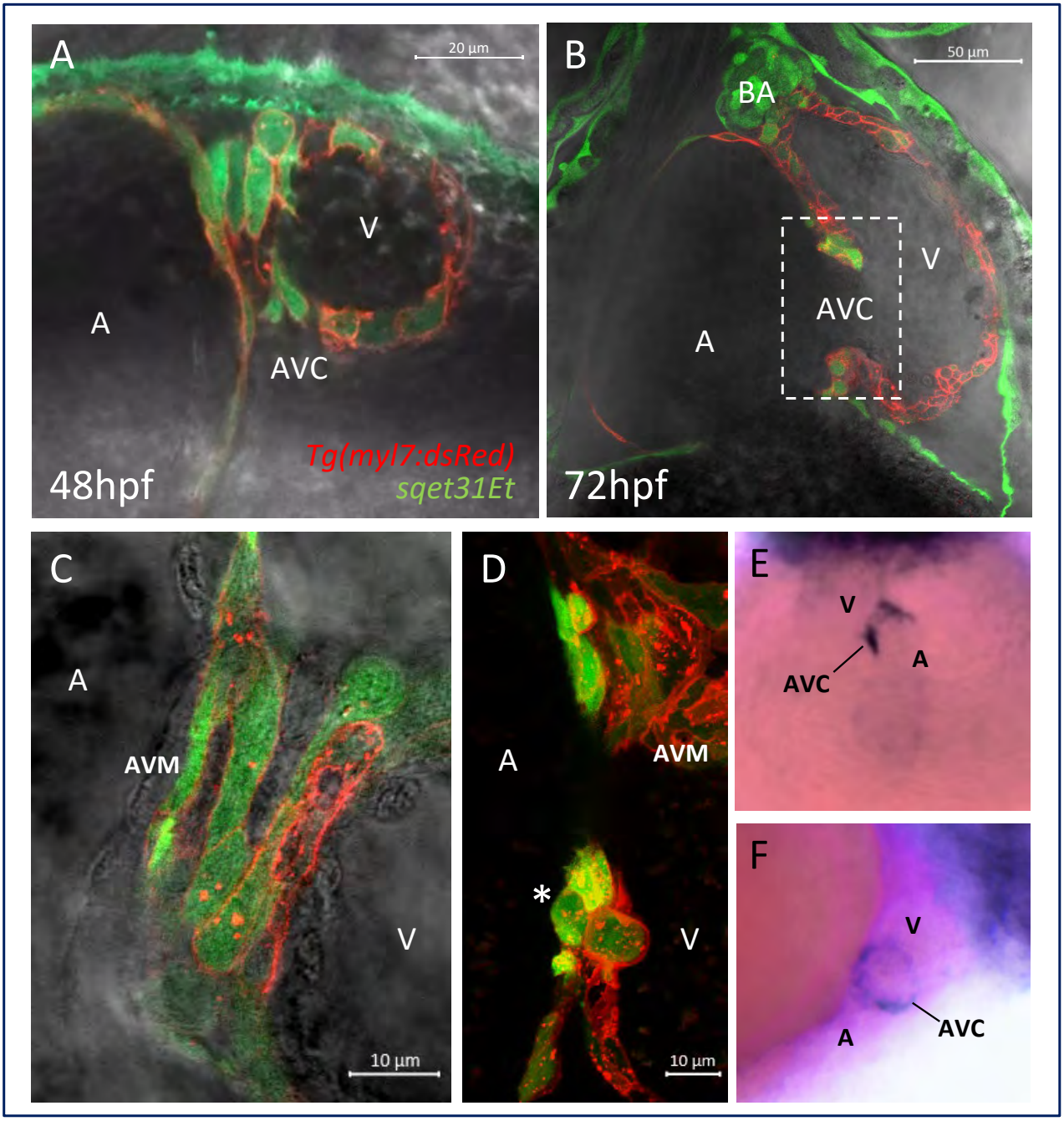

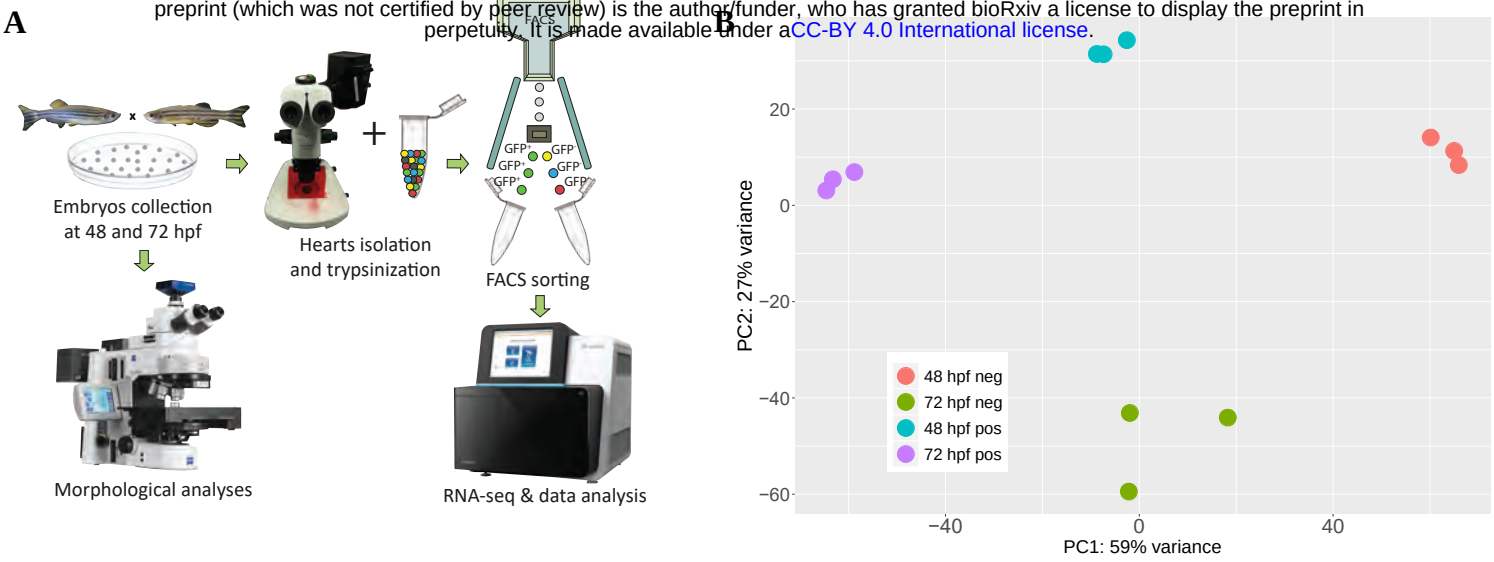

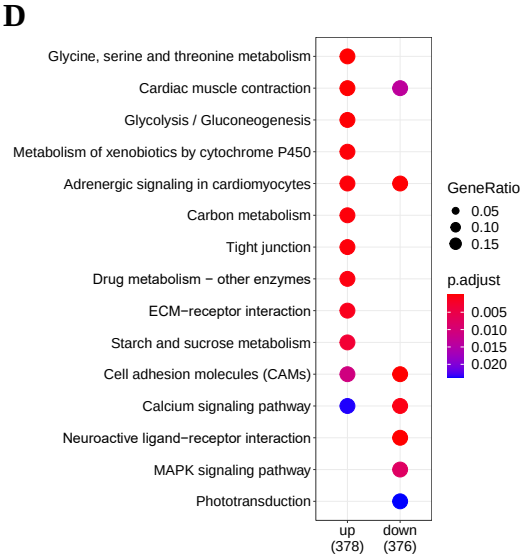

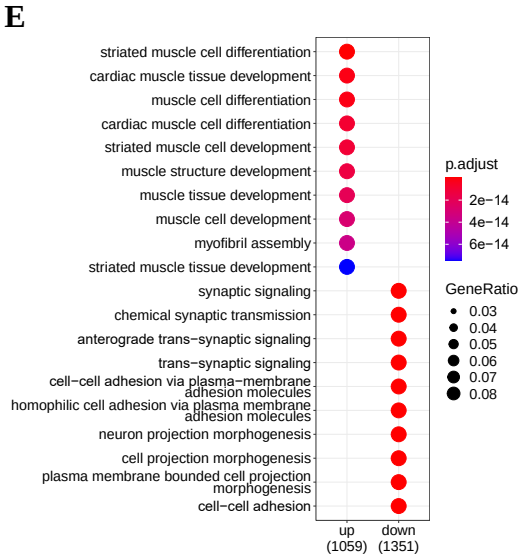

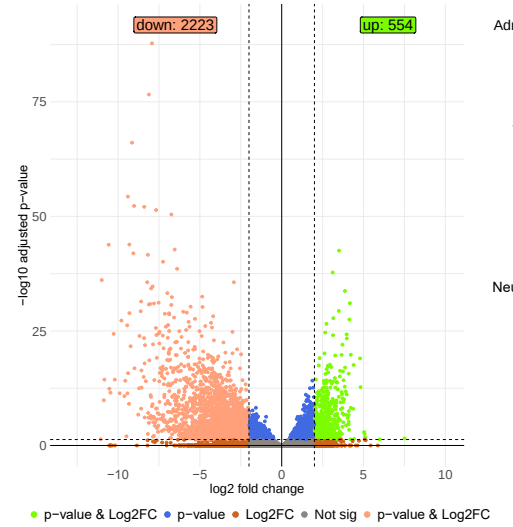

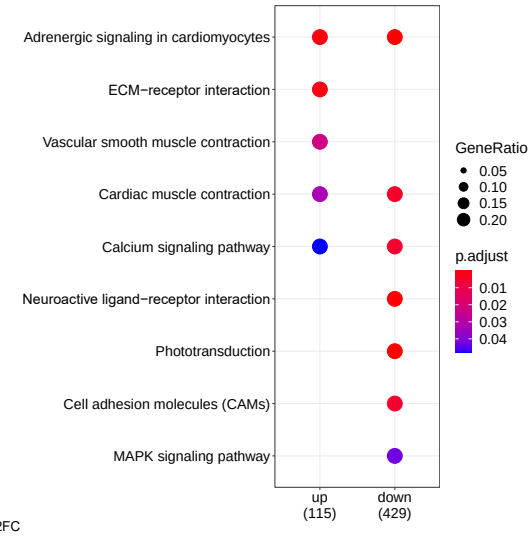

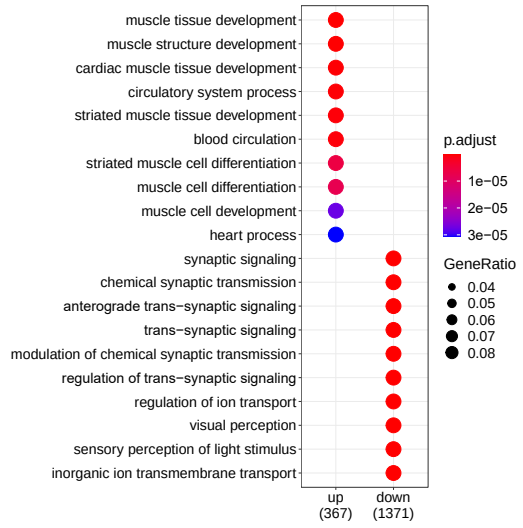

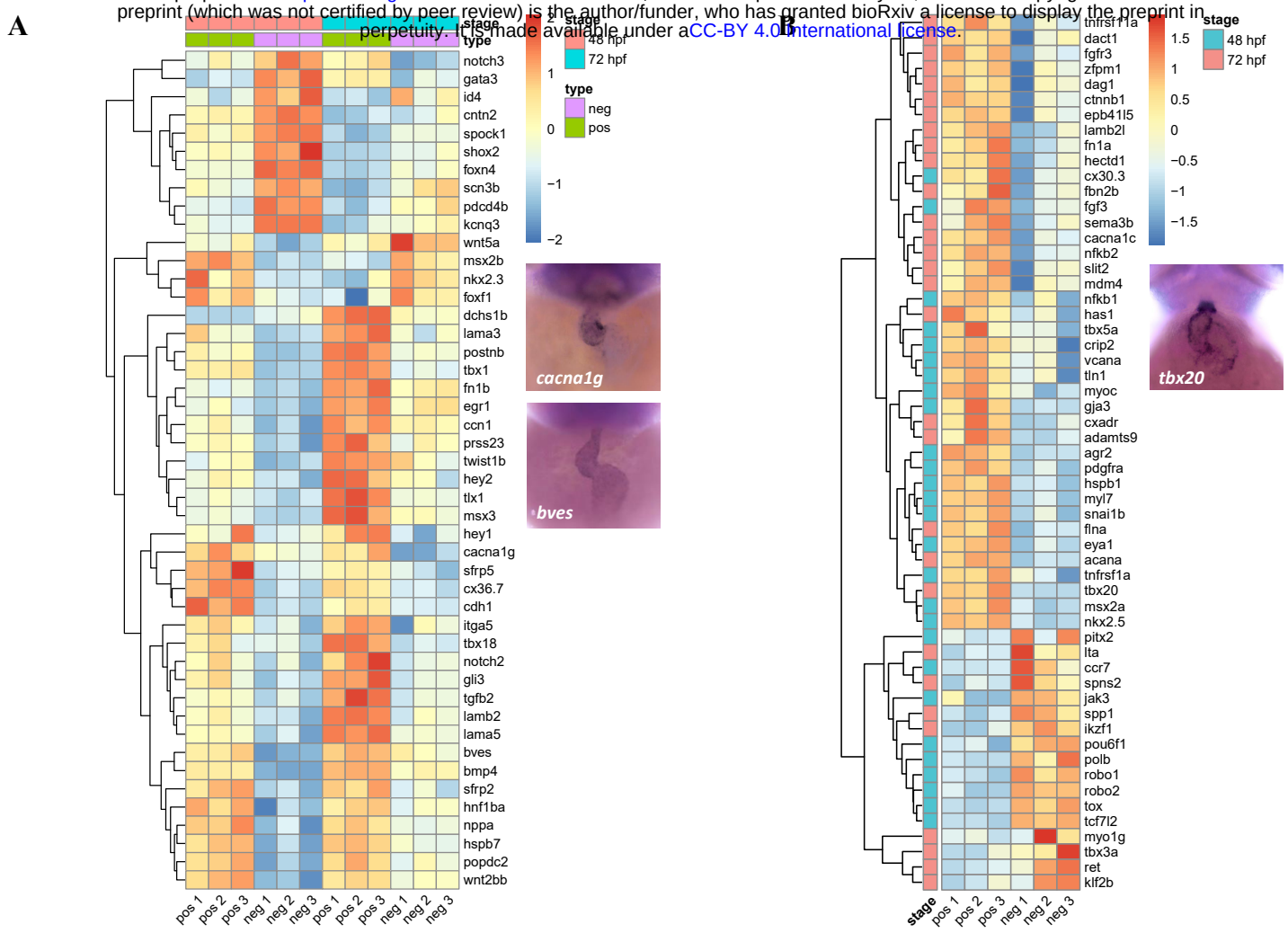

Zebrafish	Mammal	Conductance
Cx36.7	CX31.9/ Cx30.2	Ultra-low (Sultana et al., 2008; Watanabe, 2017)
Cx43.4/ Cx44.2	CX45	Low (Watanabe, 2017)
Cx28.9/ Cx32.3	CX37	Variable (Hu et al. 2006)
Cx43	CX43	Medium (Gemel et al. 2008)
Gja3	CX46	(cardiac arrhythmia, Chi et al., 2010)
Cx30.3		?
Cx34.4		?
Cx35.4		?

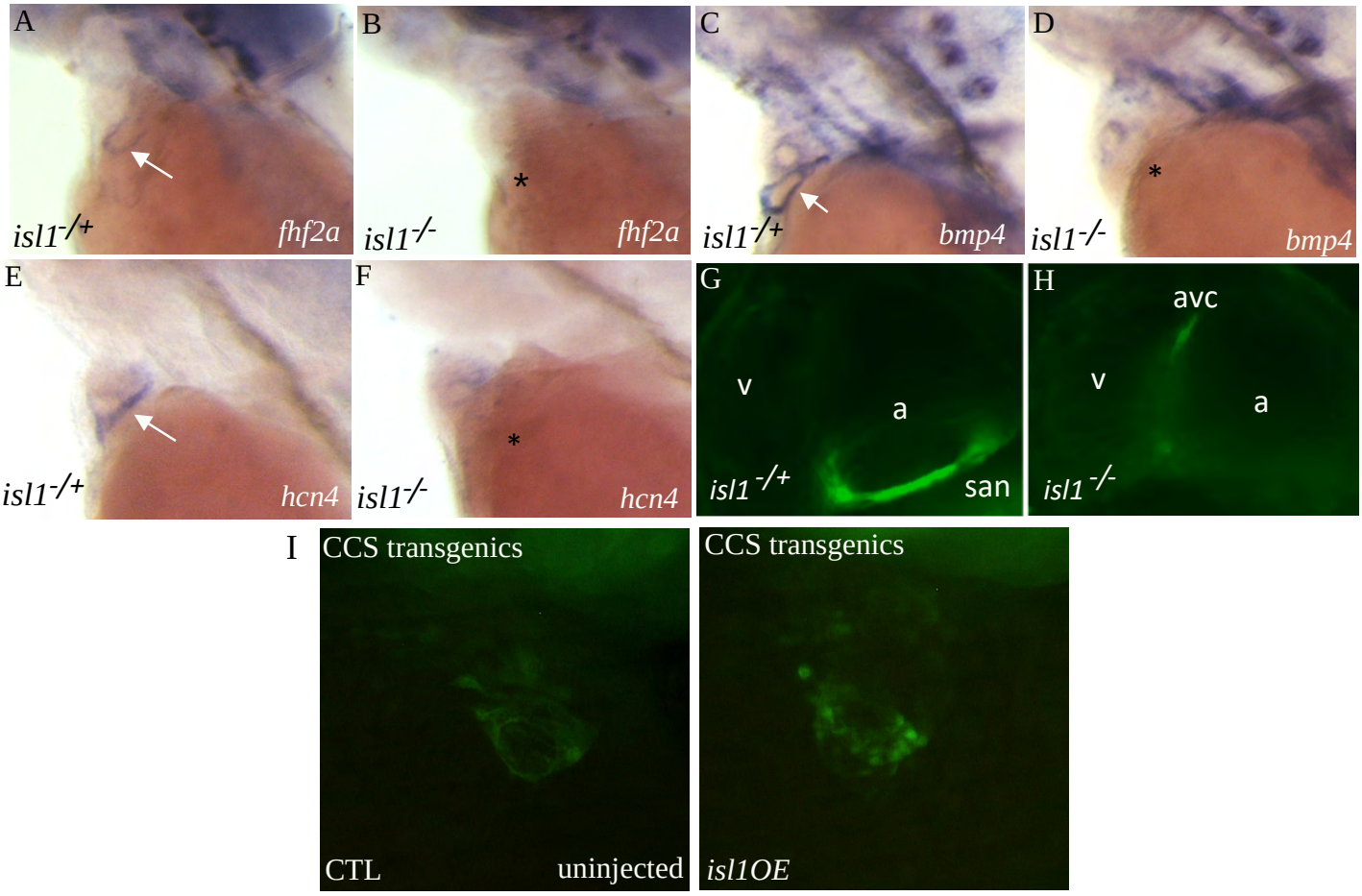

J

Fluorescence	CTL (N=9)	*isl1*OE (N=13)
Mean	13.08	16.45
SD	1.29	2.49
Min	11.62	13.20
Max	14.72	20.96

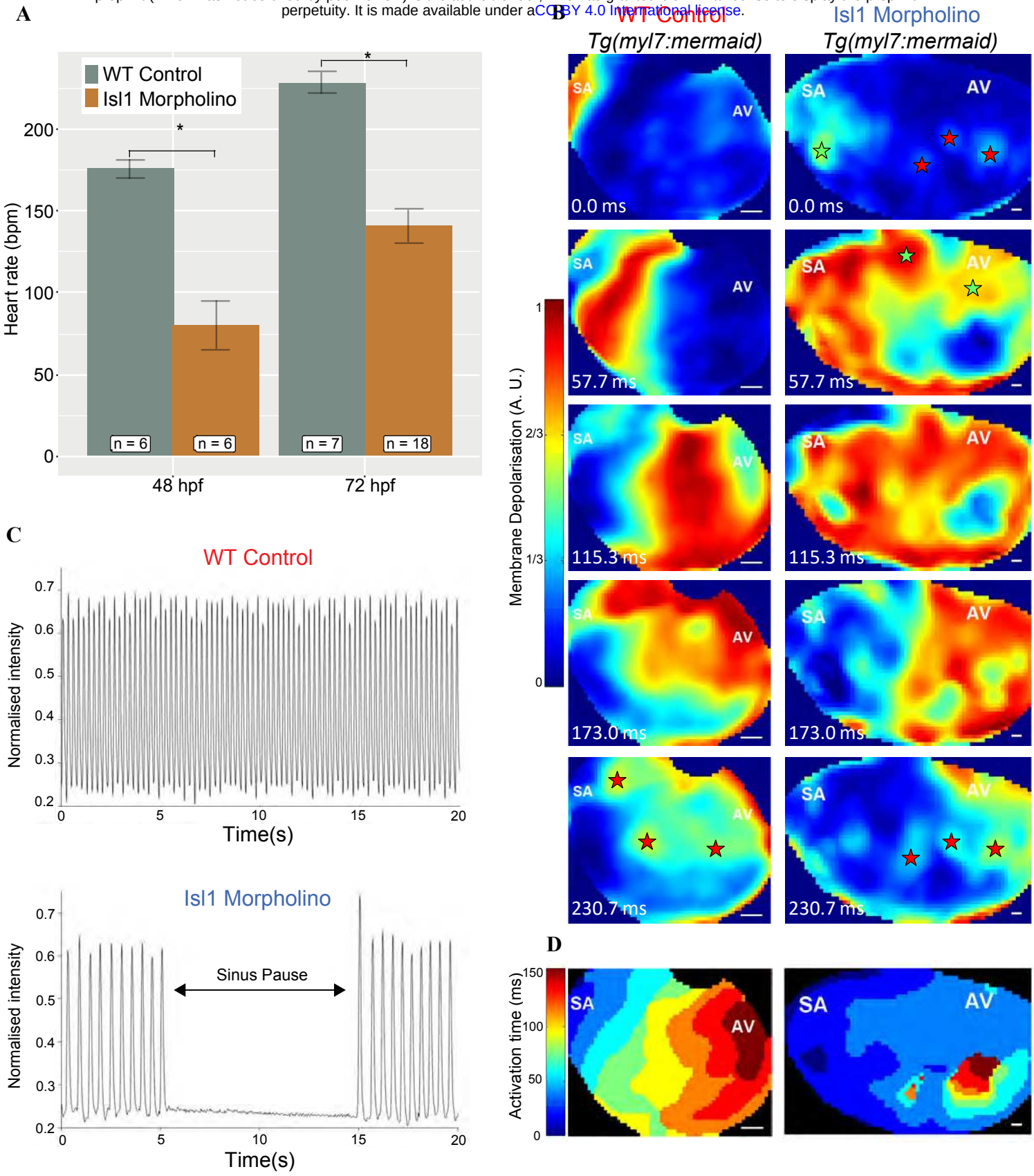

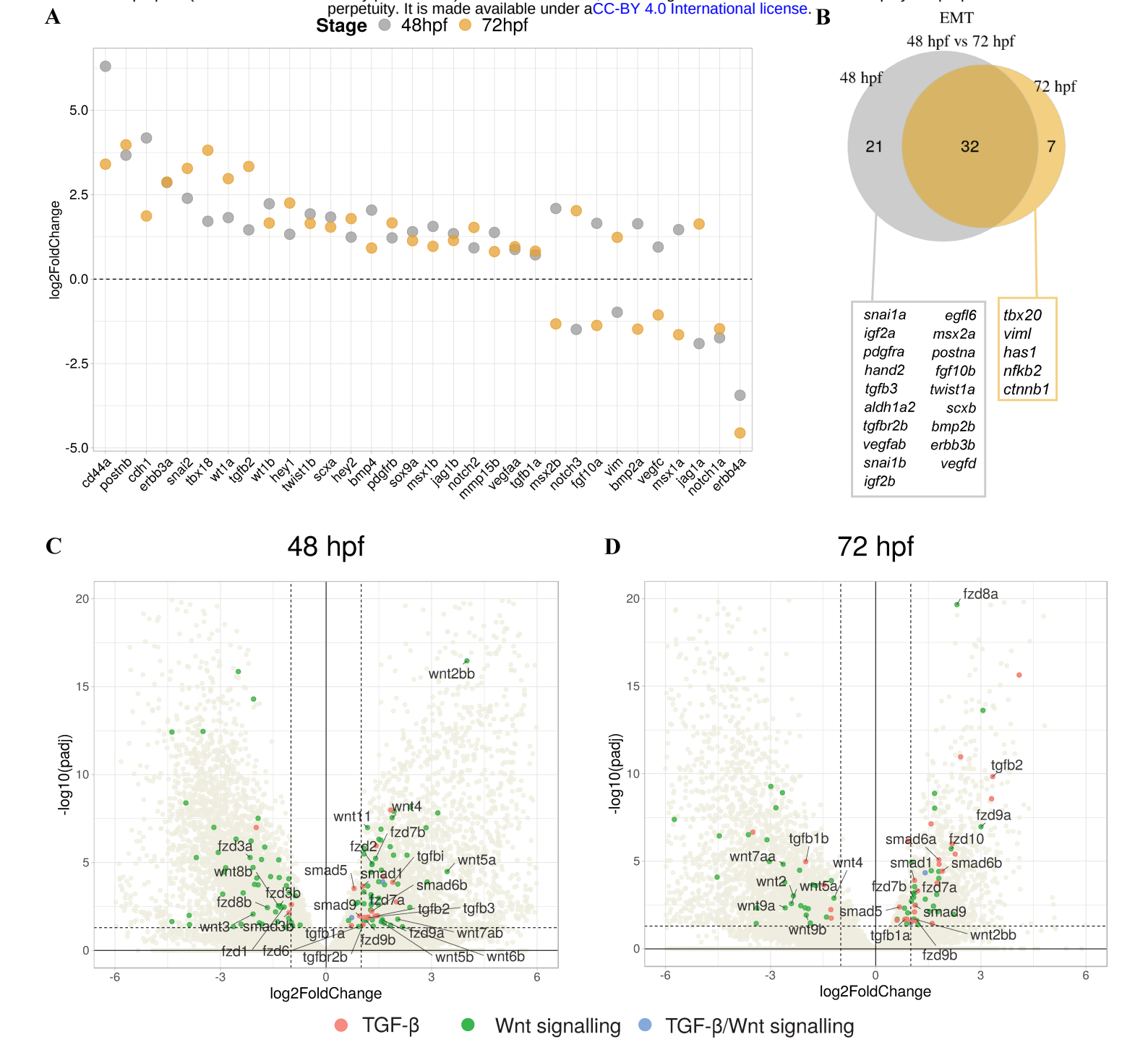

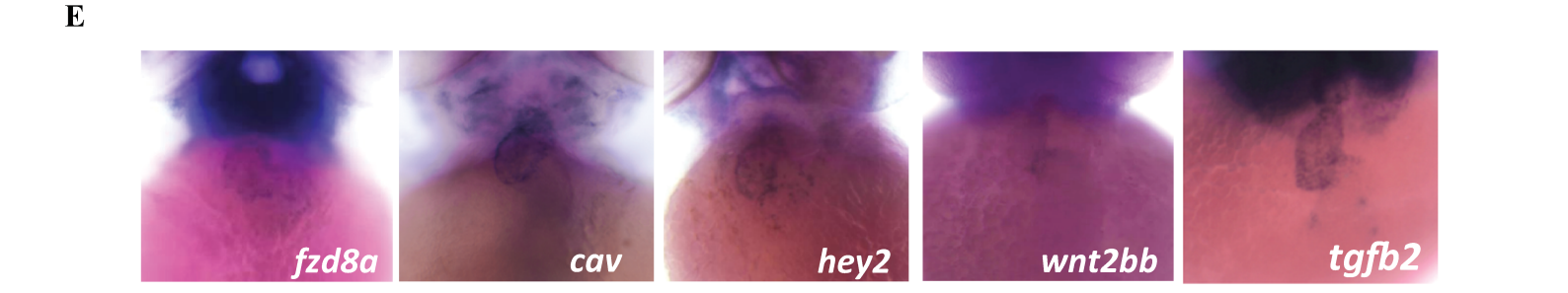

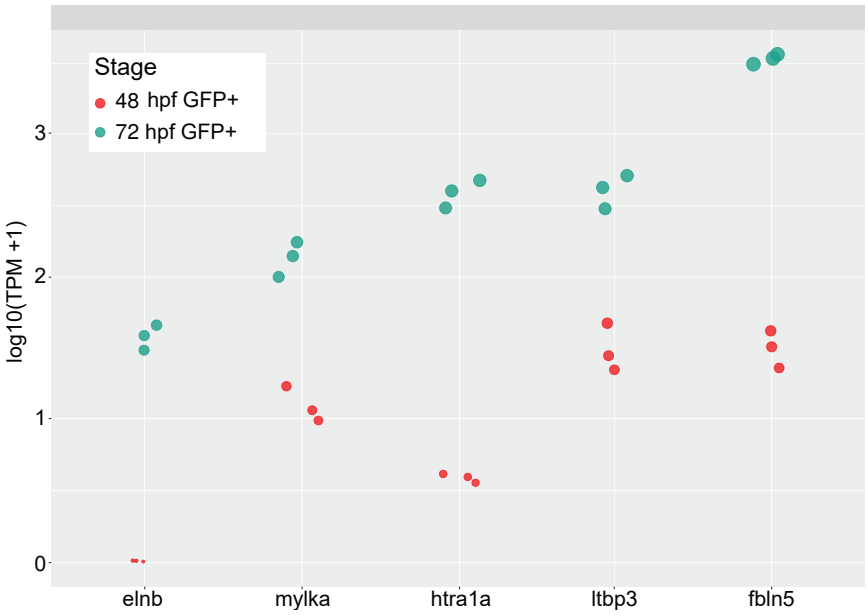

A

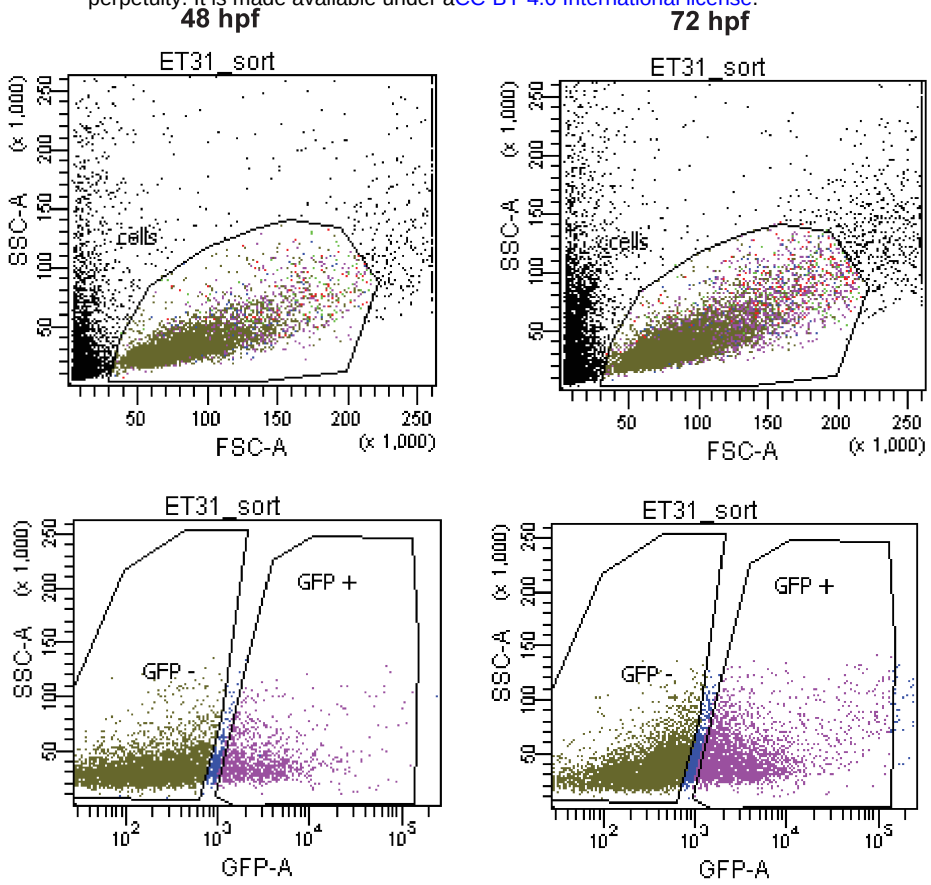

B

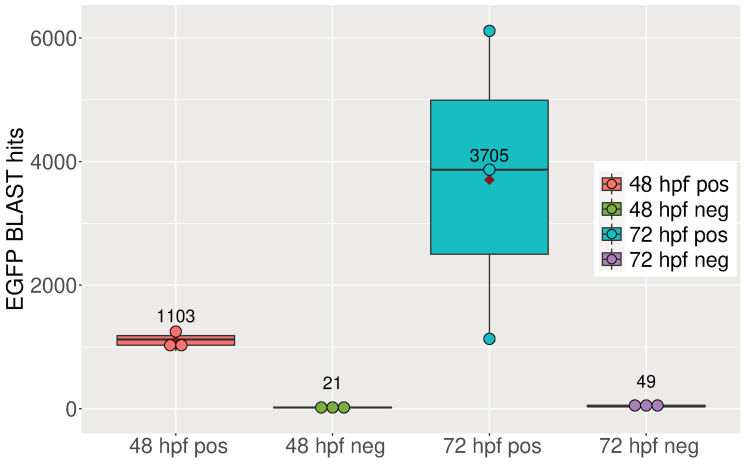

C

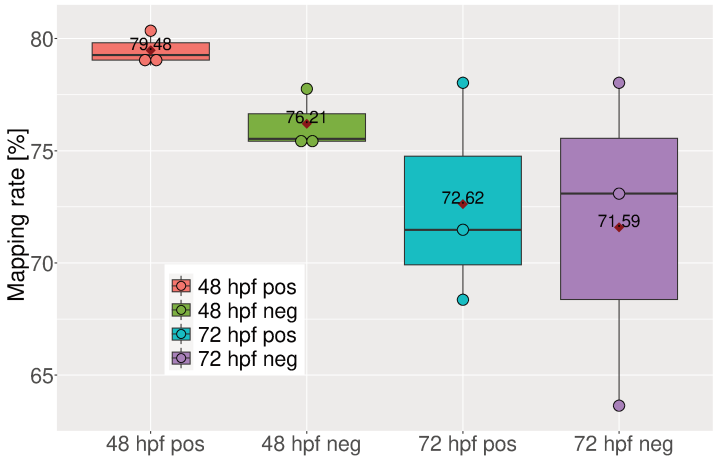

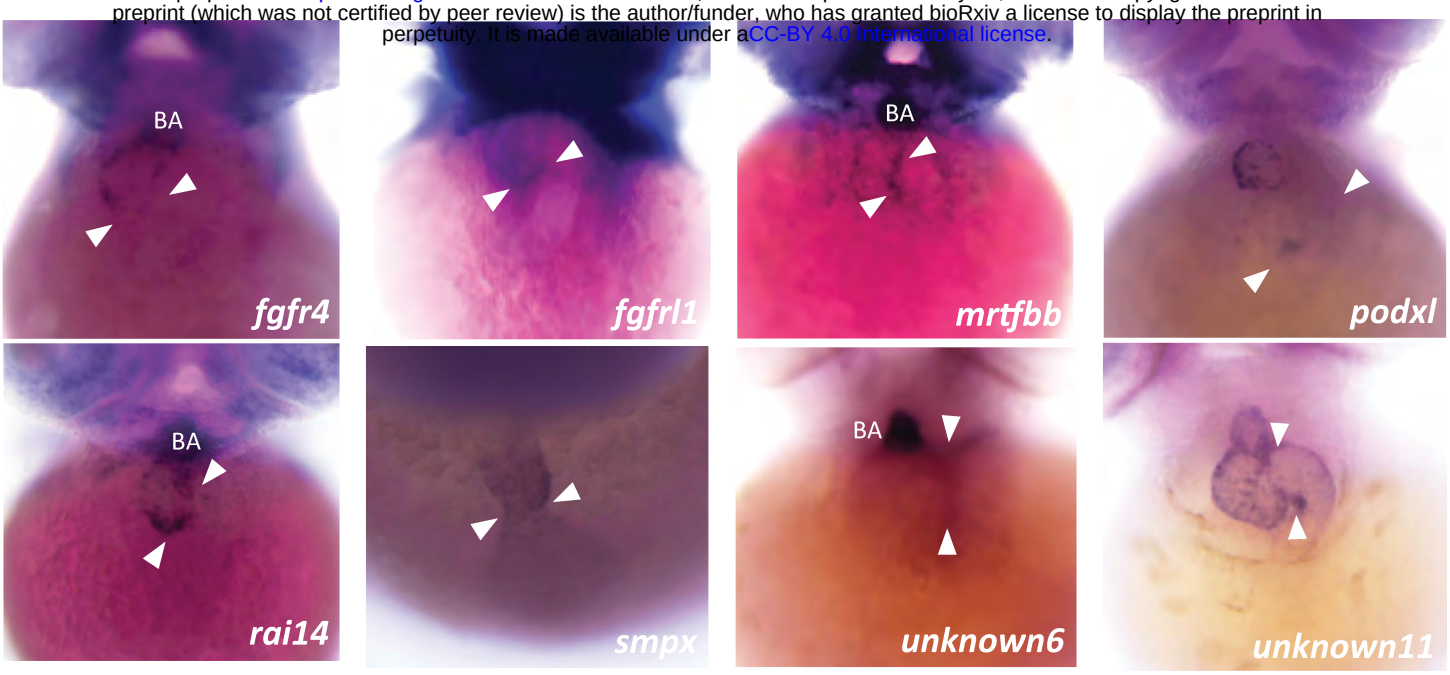

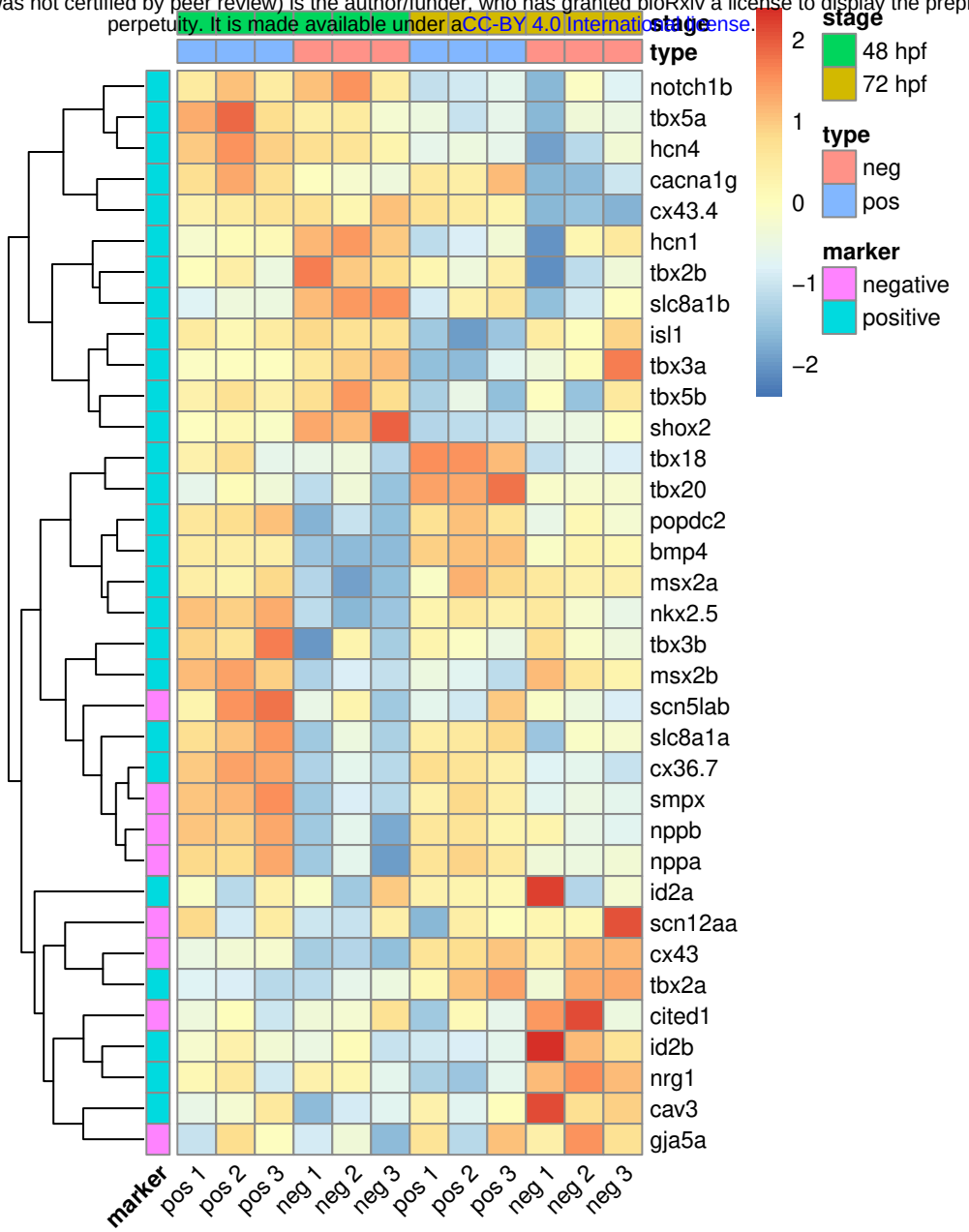

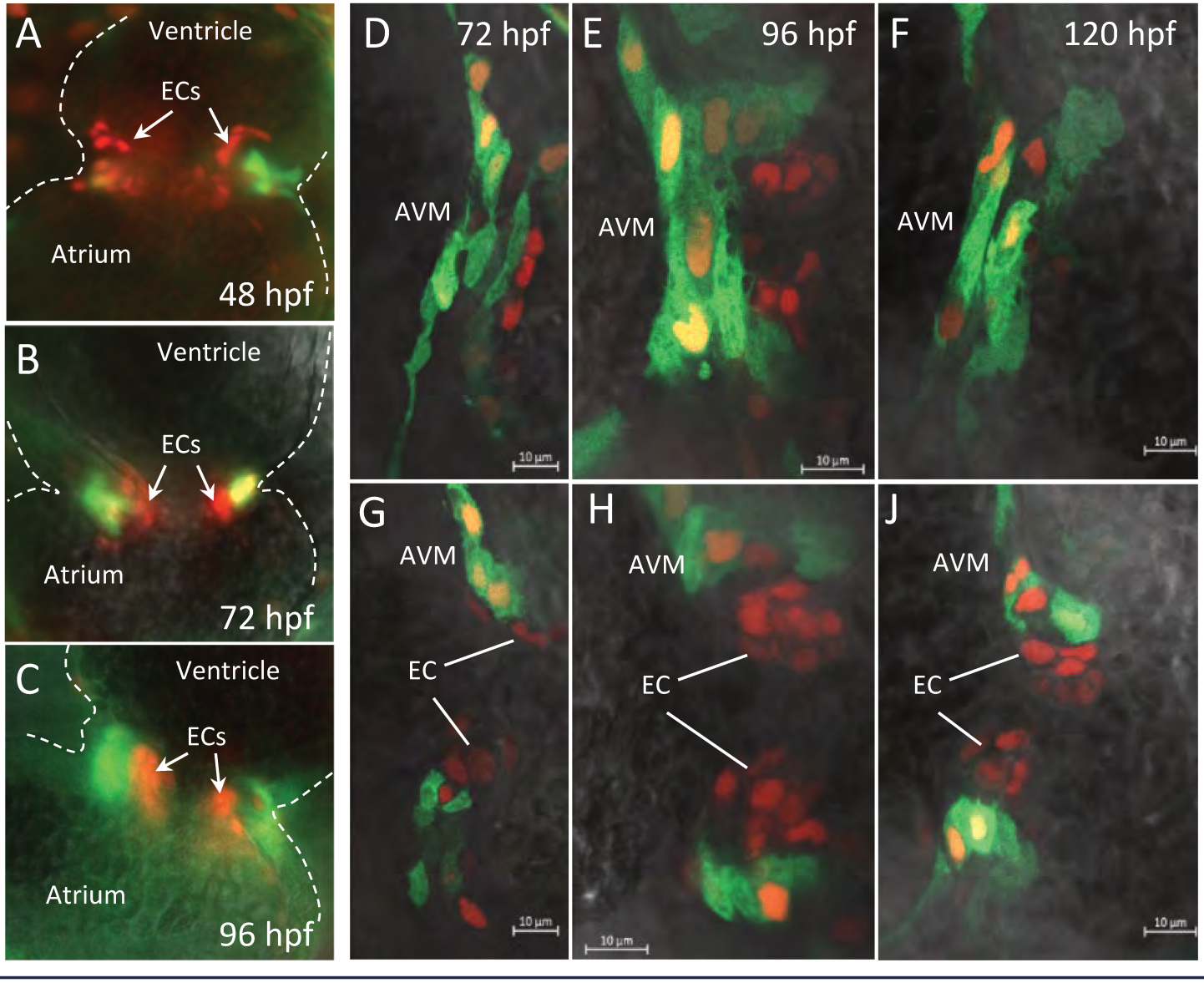

A

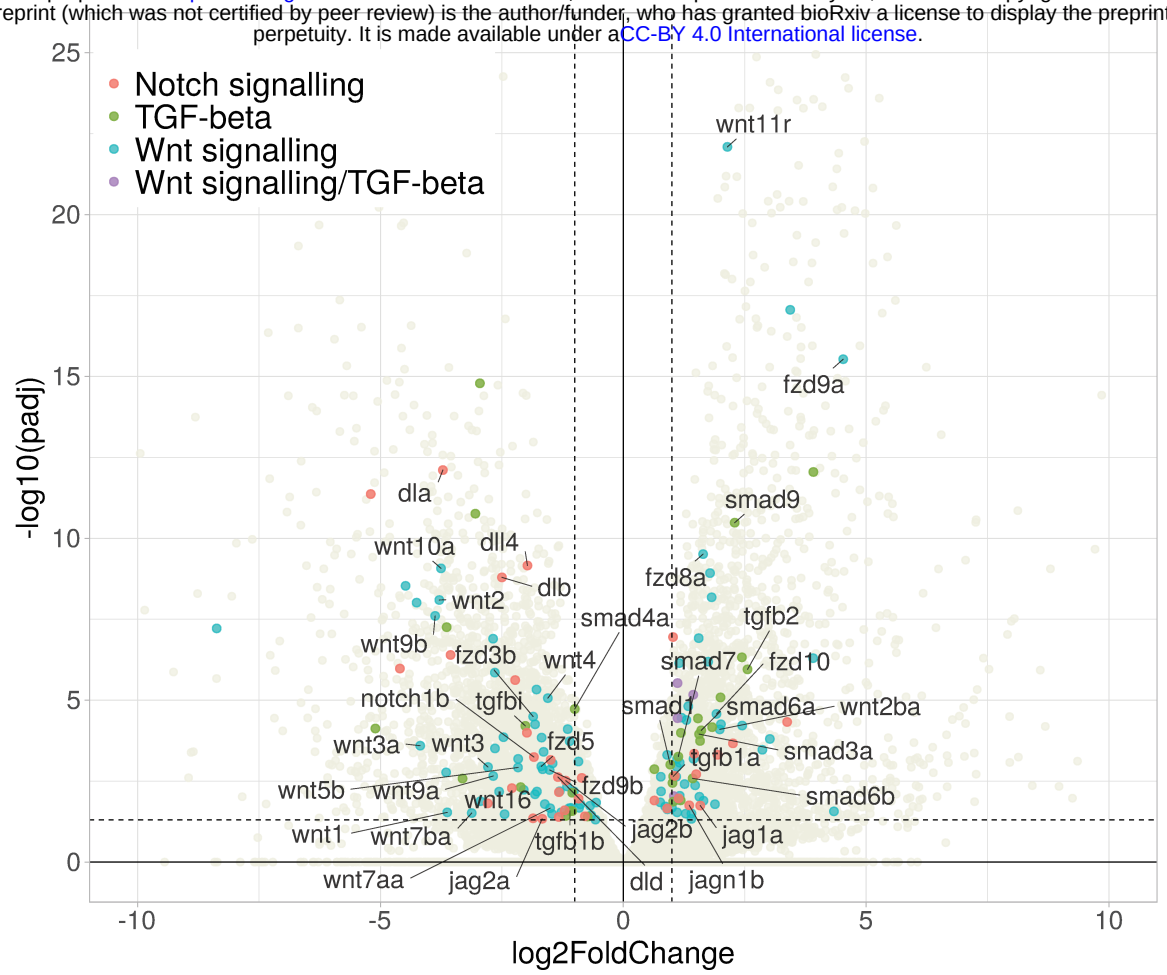

B